Forschungszentrum Karlsruhe
in der Helmholtz-Gemeinschaft

Wissenschaftliche Berichte
FZKA 6962

Stellar Neutron Capture Cross Sections of the Hf Isotopes

K. Wisshak, F. Voss, F. Käppeler, L. Kazakov, M Krtička

Institut für Kernphysik

Februar 2004

FORSCHUNGSZENTRUM KARLSRUHE
in der Helmholtz-Gemeinschaft
Wissenschaftliche Berichte
FZKA 6962

STELLAR NEUTRON CAPTURE CROSS SECTIONS OF THE Hf ISOTOPES

K. WISSHAK, F. VOSS, F. KÄPPELER, L. KAZAKOV[1], and M. KRTIČKA[2]

Institut für Kernphysik

[1]Institute for Physics and Power Engineering, Obninsk–Kaluga Region, Russia
[2] Charles University, Prague, Czech Republic

Forschungszentrum Karlsruhe GmbH, Karlsruhe
2004

Impressum der Print-Ausgabe:

Als Manuskript gedruckt

Forschungszentrum Karlsruhe GmbH
Postfach 3640, 76021 Karlsruhe

Mitglied der Hermann von Helmholtz-Gemeinschaft
Deutscher Forschungszentren (HGF)

ISSN 0947-8620

ABSTRACT

The neutron capture cross sections of ^{176}Hf, ^{177}Hf, ^{178}Hf, ^{179}Hf, and ^{180}Hf have been measured in the energy range from 3 to 225 keV at the Karlsruhe 3.7 MV Van de Graaff accelerator. Neutrons were produced via the ^{7}Li$(p,n)^{7}$Be reaction by bombarding metallic Li targets with a pulsed proton beam. Capture events were registered with the Karlsruhe 4π Barium Fluoride Detector, and the cross sections were determined relative to the gold standard. The measurements were performed on highly enriched hafnium oxide samples. The respective cross section ratios could be obtained with overall uncertainties between 0.9 and 1.8%, about a factor of five more accurate than previous data. Partial cross sections to ground and isomeric states could be experimentally identified for neutron capture in ^{176,177,178,179}Hf indicating a strong population of yet unknown isomeric states in ^{177}Hf and ^{180}Hf. This feature was further confirmed by extensive GEANT simulations, using theoretically calculated capture cascades based of the known level schemes. Maxwellian averaged neutron capture cross sections were calculated for thermal energies between $kT = 8$ keV and 100 keV. For three isotopes the results agree fairly well with a recent evaluation, while the other cases differ by 13 to 37%.

ZUSAMMENFASSUNG

DIE STELLAREN (n,γ) QUERSCHNITTE DER Hf ISOTOPE

Die Neutroneneinfangquerschnitte von ^{176}Hf, ^{177}Hf, ^{178}Hf, ^{179}Hf, und ^{180}Hf wurden am Karlsruher 3.7 MV Van de Graaff Beschleuniger im Energiebereich von 3 bis 225 keV gemessen. Neutronen wurden über die ^{7}Li$(p,n)^{7}$Be–Reaktion durch Beschuss metallischer Li–Targets mit einem gepulsten Protonenstrahl erzeugt, und Einfangereignisse mit dem Karlsruher 4π Barium Fluorid Detektor nachgewiesen. Die Messung wurde relativ zum Gold Standard-Querschnitt mittels hochangereicherter Hafniumoxyd-Proben durchgeführt. Insgesamt wurden Unsicherheiten von 0.9 bis 1.8% erreicht. Die Ergebnisse sind damit um ungefähr einen Faktor fünf genauer als die Resultate früherer Arbeiten. Für Neutroneneinfang in ^{176,177,178,179}Hf konnten im Experiment partielle Einfangquerschnitte zum Grundzustand und zu Isomeren identifiziert werden, die eine starke Bevölkerung von bisher unbekannten Isomeren in ^{177}Hf und ^{180}Hf anzeigen. Dieses Verhalten wurde zusatzlich durch umfangreiche Simulationen mit dem GEANT Programmpaket bestätigt, in denen theoretische, auf der Basis der bekannten Niveauschemata berechnete, Einfangkaskaden benutzt wurden. Die stellaren Einfangquerschnitte wurden für thermische Energien von $kT = 8$ keV bis 100 keV berechnet. Für drei der untersuchten Isotope stimmen die Ergebnisse gut mit einer neueren Evaluation überein, wogegen die anderen Werte um 13 - 37% abweichen.

Contents

1 INTRODUCTION

The present measurement of the (n,γ) cross sections of the hafnium isotopes is part of a comprehensive study with the Karlsruhe $4\pi BaF_2$ detector for investigating the isotopes of the main s-process component. So far, these measurements were concentrated on the rare earth elements (REE). Apart from Ce and Er, the relevant isotopes of all REE elements with even atomic number have been successfully investigated. At lower mass numbers measurements have been performed on the even-Z elements between Cd and Ba. These results were included in a recent update of a compilation of recommended stellar (n,γ) rates [1].

The present work on hafnium, the first element above the REE region, represents a logical extension of this concept. The s-process reaction path sketched in Fig. 1 shows that the hafnium isotopes are connecting the two elements lutetium and tantalum, which are both of special importance for s-process studies.

The s-only isotope ^{176}Hf is shielded against the β-decay chains from the r-process by its stable isobar ^{176}Yb. It is partly produced by neutron captures on ^{175}Lu feeding the short-lived isomer in ^{176}Lu ($t_{1/2} = 3.68$ h) and partly by the decay of the long-lived ^{176}Lu ground state ($t_{1/2} = 36$ Gyr). Originally the decay of the ground state was considered as a potential clock for the age of the s elements. However, it was suspected [2] and later confirmed [3] that the energetic thermal photon bath at the s-process temperatures of typically 300 MK leads to an equilibration in the population of ground state and isomer, and hence to a drastic reduction of the effective stellar half life of ^{176}Lu, thus converting the cosmic clock into a stellar thermometer. This possibility can be explored as soon as reliable stellar neutron capture cross section become available, since the solar Lu/Hf abundance ratio has been accurately determined [4].

At the other end of the hafnium isotope chain, the puzzling origin of the rarest stable isotope in nature, ^{180}Ta^m, has been intensively studied in the past decade (see Refs. [5, 6]). This isotope owes its existence to remarkable features of the Hf isotopes, namely to a sophisticated balance of β-decays from excited states and neutron capture feeding of isomeric states. This complex nuclear reaction pattern in combination with the intricate details of He shell flashes in thermally pulsing low mass AGB stars was shown to provide most or all of the ^{180}Ta^m abundance observed today [5, 7].

Fig. 1 shows that the s-process reaction path in the Lu-Hf-Ta-W region is complicated by weak branchings indicated by thin arrows. Several of these branchings are due to the population of isomeric states in the hafnium isotopes. The description of the branchings requires the separate determination of the respective partial capture cross sections feeding the ground state and the isomer. This option could only be realized in TOF measurement with the $4\pi BaF_2$ detector thanks to the combination of high efficiency and good resolution in γ-ray energy, and was first demonstrated at the example of several isomers in ytterbium [8, 9].

Cross section measurements on the hafnium isotopes are complicated by the fact that

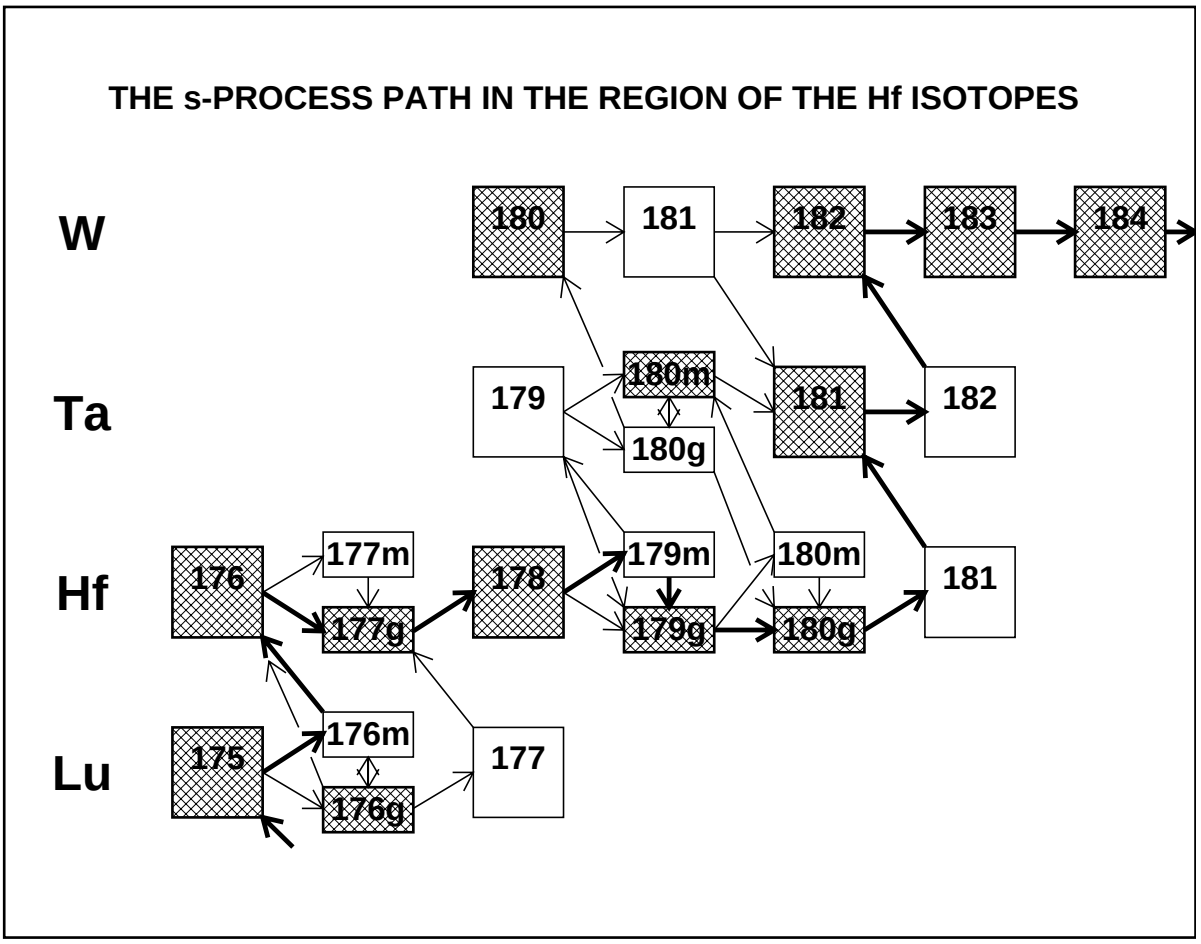

Figure 1: The reaction path of the s process in the region of the hafnium isotopes. Relevant isomeric states are indicated by separate boxes. Note that ^{176}Lu and ^{176}Hf represent s-only isotopes since they are shielded against β-decays from the r-process region by ^{176}Dy. Similarly, ^{180}Ta^m and ^{180}W are shielded by ^{180}Hf.

neutron capture may significantly populate a number of isomeric states. For conventional techniques based on Moxon-Rae type detectors or on total energy detectors with pulse height weighting, this feature implies inherent uncertainties, which are difficult to quantify. Moreover, these techniques do not allow to distinguish capture cascades feeding the ground state or the isomer, but consider the sum energy of the capture cascade - represented by the binding energy of the captured neutron plus its comparably small kinetic energy - as a fixed parameter. Accordingly, events leading to the isomer are evaluated with binding energies, that are too high. This effect may cause systematic uncertainties of the order of 10% as was recently observed for the ytterbium isotopes [10].

This concerns also the previous keV neutron capture data for hafnium, which were obtained in TOF measurements with total energy detectors [4, 11, 12]. Although uncertainties of 3% to 6% were quoted for these cross sections, these data exhibit discrepancies

of 15% to 22% for the odd isotopes ^{177}Hf and ^{179}Hf.

The present experiment aims at resolving these discrepancies on the basis of a significantly refined experimental technique. This technique allows one to achieve a much better overall accuracy and to separate the partial cross sections to isomers and to the respective ground states. The second point is facilitated by the fact that the relevant isomeric states occur at excitation energies well above 250 keV. Hence, the resolution in γ-energy of the 4πBaF$_2$ detector suffices to distinguish capture cascades to the isomers from those to the ground states.

The measurements and the main part of data analysis are described in Secs. 2 and 3. Sec. 4 deals with complementary computer simulations and with the determination of isomeric ratios. The final differential cross sections and the related uncertainties are discussed in Secs. 5 and 6, followed by the resulting Maxwellian averaged stellar cross sections in Sec. 7. The astrophysical implications of the new data will be addressed in a forthcoming publication.

2 EXPERIMENT

The neutron capture cross sections of the hafnium isotopes 176 to 180 have been measured in the energy range from 3 to 225 keV using gold as a standard. Since the experimental method has been published in detail [13, 14, 15, 16], only a general description is given here, complemented with the specific features of the present measurement.

Neutrons were produced via the ^{7}Li$(p,n)^7$Be reaction by bombarding metallic Li targets with the pulsed proton beam of the Karlsruhe 3.7 MV Van de Graaff accelerator. The neutron energy was determined by time of flight (TOF), the samples being located at a flight path of 79 cm. The relevant parameters of the accelerator were a pulse width of $<$1 ns, a repetition rate of 250 kHz, and an average beam current of 2.0 μA. In different runs, the proton energies were adjusted 30 keV and 100 keV above the threshold of the ^{7}Li$(p,n)^7$Be reaction at 1.881 MeV. In this way, continuous neutron spectra in the proper energy range for s–process studies were obtained, ranging from 3 keV to 100 keV, and from 3 keV to 225 keV, respectively. The lower maximum neutron energy offers a significantly better signal-to-background ratio at low energies.

Capture events were registered with the Karlsruhe 4π Barium Fluoride Detector via the prompt capture γ–ray cascades. This detector consists of 42 hexagonal and pentagonal crystals forming a spherical shell of BaF$_2$ with 10 cm inner radius and 15 cm thickness. It is characterized by a resolution in γ–ray energy of 7% at 2.5 MeV, a time resolution of 500 ps, and a peak efficiency of 90% at 1 MeV. The 1.5 MeV threshold in γ–ray energy used in the present experiment corresponds to an efficiency for capture events of more than 95% for all investigated isotopes. A comprehensive description of this detector can be found in Ref. [15].

The experiment was divided into three runs, two using the conventional data acquisition technique with the detector operated as a calorimeter, and one with an analog-to-digital converter (ADC) system for analyzing the signals from all modules individually. In this way, the full spectroscopic information can be recovered.

The hafnium samples were prepared from isotopically enriched oxide powder (HfO$_2$),

which was heated to 1200 K for 15 min to eliminate water contaminations. Then the various batches were pulverized in an agate mortar, pressed into pellets 15mm in diameter and reheated to 1200 K for 1 h. During the final heating the pellets shrank slightly. Immediately after cooling, the actual samples were prepared by canning the pellets into air tight aluminum cylinders with 0.2 mm thick walls. Apart from the five hafnium samples, a gold sample in an identical can was used for measuring the neutron flux. An empty can was mounted in the sample ladder for determining the sample-independent background. A graphite sample served for simulating the background due to scattered neutrons. The relevant sample parameters are compiled in Table 1, and the isotopic composition of the hafnium samples provided by IPPE Obninsk is listed in Table 2.

Table 1: SAMPLE CHARACTERISTICS

Sample	Diameter	Thickness		Weight	Can[b]	Neutron binding
	(mm)	(mm)	(10^{-3}at/barn)[a]	(g)	(g)	energy (MeV)
^{178}Hf[c]	14.8	3.5	4.1930	2.5842	0.311	6.100
Graphite	15.0	2.0	17.628	0.6213	0.187	
^{177}Hf	14.9	0.9	1.1425	0.7013	0.274	7.626
^{176}Hf	15.1	3.2	4.2132	2.5791	0.318	6.383
^{197}Au	15.0	0.4	2.2485	1.2996	0.258	6.513
^{179}Hf	14.9	1.4	1.6101	0.9975	0.275	7.388
Empty	15.0				0.278	
^{180}Hf[c]	14.9	5.0	6.4176	3.9905	0.362	5.696

[a]For hafnium samples: sum of all Hf isotopes
[b]Aluminum cylinder
[c]Corresponding to sample order of run I. In runs II and III, the positions of the ^{178}Hf and ^{180}Hf samples were exchanged

Table 2: ISOTOPIC COMPOSITION (in %)

Sample	Isotope				
	^{176}Hf	^{177}Hf	^{178}Hf	^{179}Hf	^{180}Hf
^{176}Hf	64.60	21.70	6.80	2.20	4.70
^{177}Hf	1.10	82.80	13.60	1.00	1.50
^{178}Hf	0.80	1.90	92.40	3.30	1.60
^{179}Hf	0.20	1.50	4.60	73.70	20.00
^{180}Hf	0.20	0.80	2.20	2.50	94.30

The neutron transmission of the samples calculated with the SESH code [17] was generally larger than 90% (Table 3). The measured spectra of all samples were normalized to equal neutron flux by means of a ^{6}Li–glass monitor located close to the neutron target. The transmission spectra measured with a second ^{6}Li–glass detector at a flight path of

260 cm were used for a rough determination of the total cross sections. Though the accuracy of this method is inferior to that obtained in a dedicated experiment, these total cross sections can be used in the calculation of the multiple scattering correction.

The samples were moved cyclically into the measuring position by a computer controlled sample changer. The data acquisition time per sample was about 10 min, a complete cycle lasting about 1.3 h. From each event, a 64 bit word was recorded on DLT tape containing the sum energy and TOF information together with 42 bits identifying the contributing detector modules. The respective parameters of the three runs corresponding to neutron spectra with different maximum energies are listed in Table 4. The data in run II were recorded with the ADC system.

Table 3: CALCULATED NEUTRON TRANSMISSION[a]

Sample	Neutron Energy (keV)				
	10	20	40	80	160
^{197}Au	0.959	0.965	0.970	0.974	0.979
^{176}Hf	0.908	0.918	0.925	0.931	0.937
^{177}Hf	0.974	0.978	0.981	0.984	0.986
^{178}Hf	0.912	0.920	0.927	0.934	0.940
^{179}Hf	0.965	0.969	0.971	0.974	0.976
^{180}Hf	0.875	0.884	0.891	0.900	0.908

[a] Monte Carlo calculation with SESH code [17].

Table 4: PARAMETERS OF THE INDIVIDUAL RUNS

Run	Flight Path (mm)	TOF Scale (ns/ch)	Number of Cycles	Maximum Neutron Energy (keV)	Measuring Time (d)	Mode of Operation	Average Beam Current (μA)	Threshold in Sum Energy (MeV)
I	788.1	0.7603	385	100	19.7	Calorimeter	2.0	1.6
II	786.5	0.7079	260	100	16.5	ADC	1.6	1.5
III	788.1	0.7431	166	200	9.3	Calorimeter	2.2	1.5

3 DATA ANALYSIS

3.1 Total Cross Sections

The total cross sections of the investigated isotopes were determined in the neutron energy range from 10 to 200 keV via the TOF spectra measured with the ^{6}Li glass detector at a flight path of 260 cm. The total cross sections and the related uncertainties were obtained as described in Ref. [13], and are listed in Table 5. The results deduced for the carbon sample agree within $\pm$5.0% with the data from the Joint Evaluated File (JEF) [18] in the

energy range from 15 to 100 keV, except in two bins from 30 keV to 40 keV and from 80 keV to 90 keV where the present data are significantly smaller because of the strong aluminum resonances of the sample cans at 34 and 87 keV. As can be seen from Table 1 the mass of the can for the graphite sample was significantly lower than that of all other cans. This leads to an overcompensation of the effect due to neutron scattering on the aluminum can of the graphite sample in the corresponding bins and, consequently to systematically underestimated total carbon cross sections.

The quoted uncertainties were obtained under the assumption that they are inversely proportional to the fraction of neutrons interacting in the sample, $A = 1 - T$, where T is the transmission. For the carbon sample this fraction is $A = 7.2\%$, the related uncertainty of 5.0% being estimated from the comparison with the JEF data. The cross section for elemental hafnium, which was calculated from the isotopic contributions with the assumption that the rare isotope ^{174}Hf has the same cross section as ^{176}Hf, was found in reasonable agreement with the data given in Ref. [19]. However, the present data are systematically lower by $\sim 10\%$ compared to the ENDF/B-V evaluation, but still compatible with the quoted uncertainties.

Table 5: MEASURED TOTAL CROSS SECTIONS [a]

Neutron Energy	Total Cross Section (barn)						
(keV)	^{176}Hf	^{177}Hf	^{178}Hf	^{179}Hf	^{180}Hf	^{12}C	^{197}Au
10 – 15	13.7	21.1	13.7	10.8	13.7	4.30	14.4
15 – 20	12.0	16.4	14.2	11.7	12.5	4.32	16.1
20 – 30	11.4	16.6	13.0	15.3	10.7	4.42	14.2
30 – 40	12.5	10.3	11.0	11.2	10.8	3.55	12.6
40 – 60	11.6	11.1	10.8	10.3	10.2	4.35	12.0
60 – 80	9.6	11.2	10.2	8.8	10.0	4.30	10.6
80 – 100	10.1	7.7	8.6	8.0	8.3	3.54	9.1
100 – 150	10.4	8.0	9.3	7.8	8,6	3.87	10.0
150 – 200	9.8	9.2	9.6	9.1	8.3	3.79	8.8
Typical Uncertainty (%)	8.0	23.5	7.3	21.9	5.4	5.0	12.8

[a] Determined from the count rate of the ^{6}Li glass neutron monitor at 260 cm flight path

3.2 Capture Cross Sections

The analysis was carried out in the same way as described previously [13, 14, 16]. All events were sorted into two–dimensional spectra containing 128 sum energy versus 2048 TOF channels according to different multiplicities (evaluation 1). In evaluation 2, this procedure was repeated by rejecting those events, where only neighboring detector modules contributed to the sum energy signal. With this option, background from the natural radioactivity of the BaF_2 crystals and from scattered neutrons can be reduced. For all samples, the resulting spectra were normalized to equal neutron flux using the count rate of the ^{6}Li glass monitor close to the neutron target. The corresponding normalization

factors are below 0.5% for all runs. The treatment of the two-dimensional spectra from the data recorded with the ADC system is slightly more complicated and was performed as described in Ref. [13].

In the next step of data analysis, sample-independent backgrounds were removed by subtracting spectra measured with the empty can. A remaining constant background was determined at very long flight times, where no time-correlated events are expected. The resulting two-dimensional spectra for events with multiplicity >2 measured in run II are shown for all investigated isotopes in Figs. 2, 3, and 4. Note that events with low sum energy and large TOF are suppressed by a preprocessing option of the ADC system.

At this point, the spectra contain only events correlated with the sample. The next correction to be made is for isotopic impurities (see Ref.[13] for details) according to the isotope matrix compiled in Table 6. The relative contributions of isotopic impurities are shown in the TOF spectra of Fig. 5. The largest correction of about 35% is obtained for the ^{176}Hf sample. This effect is much smaller for the other samples, partly because of the higher enrichment and partly because the cross sections of the impurities were smaller than that of the main isotope.

The present correction for isotopic impurities [20] holds exactly if all samples are equal in weight. Only then, second order effects due to neutron multiple scattering and self-absorption are properly accounted for. For the ^{176}Hf sample, however, the large correction for the 21.7% admixture of ^{177}Hf was complicated since the weight of the two samples differs by a factor of 3.7. Calculation of this correction directly from from the isotope matrix tends, therefore, to an overestimate due to the smaller self-shielding effect in the thin ^{177}Hf sample. Thanks to the good energy resolution of the 4π BaF_2 detector this effect can be verified in the corrected sum-energy spectrum of ^{176}Hf, where a clear dip is obtained at the binding energy of ^{177}Hf as shown in the upper right panel of Fig. 6.

This overcompensation was removed by reducing the respective correction factor of 96% (see Table 6) to 77.6, 80.9 and 81,1% for runs I,II, and III,respectively. These new factors were calculated for each run individually in such a way that the average in the region of the full energy peak for neutron capture in ^{177}Hf in the final spectrum is zero, as shown in the lower right part of Fig. 6. With this procedure, the isotopic correction is improved but still not perfect. Obviously the position of the full energy peak for capture in ^{177}Hf is not exactly at the same position in the original spectrum of the ^{176}Hf sample. Therefore, a little bump remains in the corrected spectrum above the full energy peak (lower panel of Fig. 6). This bump is exactly at the position of the full energy peak of the ^{179}Hf sample, therefore, it was suspected that it might be due to an insufficient correction of the ^{179}Hf impurity. It turned out, however, that it would be necessary to increase the ^{179}Hf impurity in the sample from 2.2% (see Table 2) to 9.3% in order to eliminate the bump from the spectrum. This possibility is, also in view of the abundance pattern of the Hf isotopes, very unlikely and was therefore discarded.

The next correction is required for the background due to capture of sample scattered neutrons in and near the detector. This component was obtained from the spectra measured with the scattering sample. The binding energy of all investigated hafnium isotopes is low enough, that the correction can be normalized via the pronounced peak in the sum-energy spectra at 9.1 MeV, which is due to capture in the odd barium isotopes ^{133}Ba and ^{135}Ba (Figs. 2 to 4).

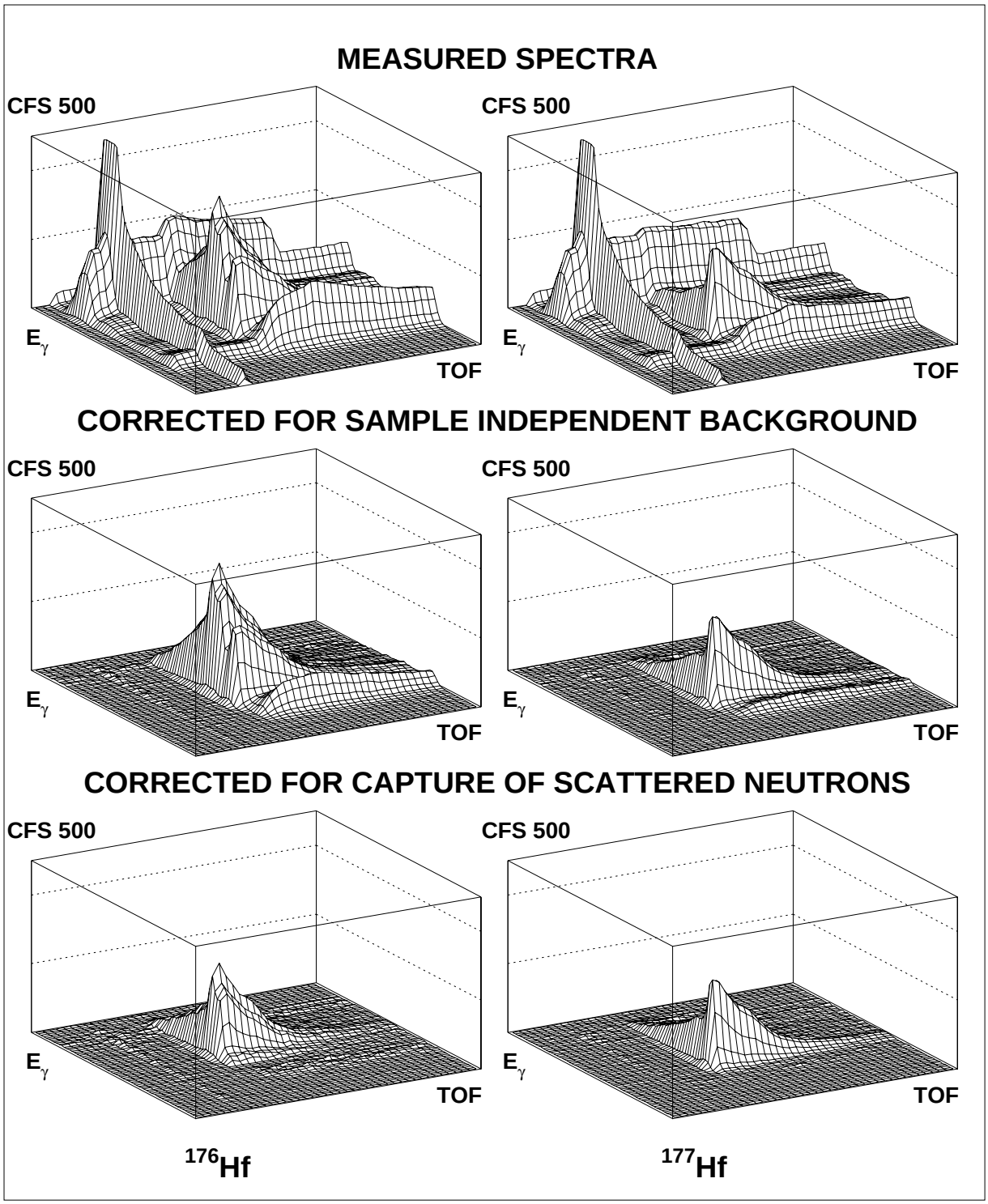

Figure 2: The different steps of background subtraction in the two–dimensional sum energy × TOF spectra. The data shown for ^{176}Hf and ^{177}Hf were measured with the ADC system in run II with 100 keV maximum neutron energy. Only events with multiplicity >2 were considered. (The original resolution of 128 × 2048 channels was compressed into 64 × 64 channels for better readability. Events at low sum-energy and large TOF are eliminated by the preprocessing option of the ADC system.)

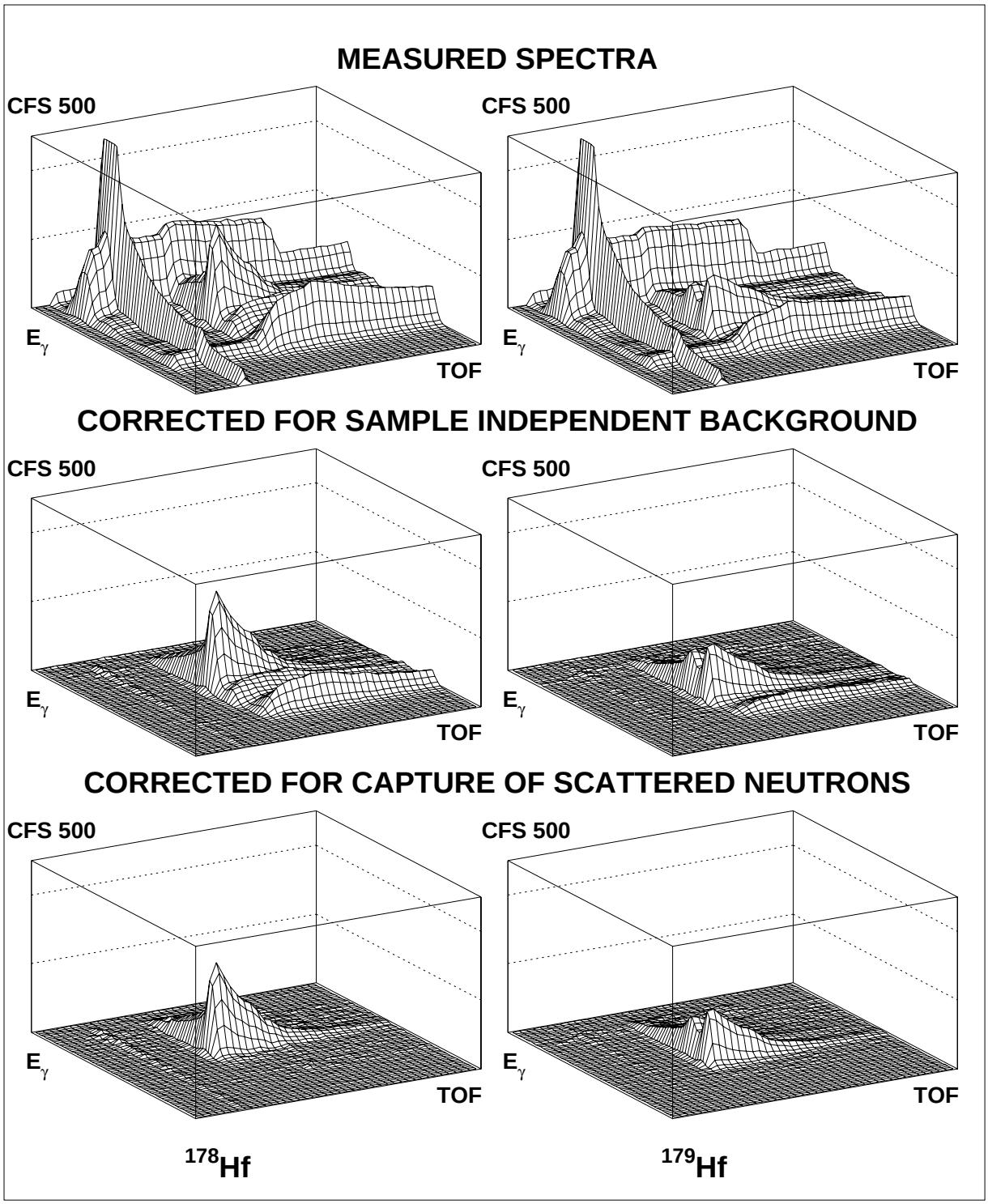

Figure 3: As Fig. 2, but for the ^{178}Hf and ^{179}Hf samples.

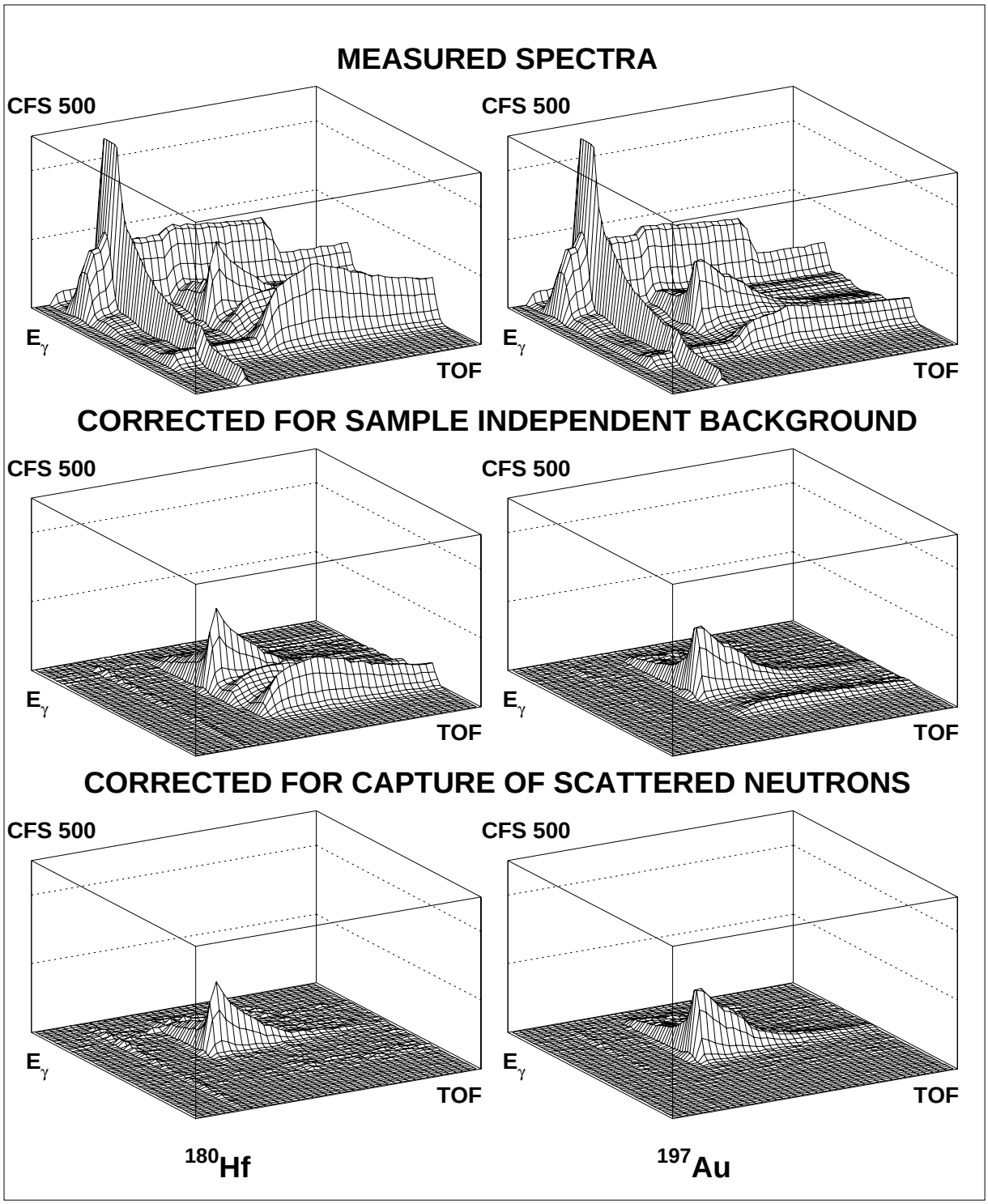

Figure 4: As Fig. 2, but for the ^{180}Hf and ^{197}Au samples.

After this last correction, the final spectra contain only the net capture events of the investigated isotopes (bottom spectra in Figs. 2, 3, and 4). The corrections for capture of scattered neutrons are shown for all measured isotopes in Fig. 7, and the corresponding signal/background ratios are listed for different neutron energies in Table 7.

After subtraction of the scattering background the cross sections as a function of neutron energy were determined from the TOF spectra of Fig. 7. These spectra are calculated by integrating the two-dimensional spectra in a region around the full energy peak. Due to the different background conditions in the spectra of events with different multiplicities, this range was chosen to decrease with multiplicity (see Fig. 9). For normalization, the two–dimensional data were projected onto the sum energy axis using the TOF region

Table 6: MATRIX FOR ISOTOPIC CORRECTIONS (%)

Corrected spectrum	Measured spectrum					Corrected sample thickness
	^{176}Hf	^{177}Hf	^{178}Hf	^{179}Hf	^{180}Hf	(10^{-3} at/barn)
^{176}Hf	100	–96.069	–3.329	–6.142	–2.636	2.6980
^{177}Hf	–0.412	100	–3.964	–0.441	–0.202	0.9388
^{178}Hf	–1.184	–6.961	100	–11.441	–0.441	3.8510
^{179}Hf	–0.064	–2.067	–1,631	100	–5.295	1.1756
^{180}Hf	–0.397	–4.442	–3.187	–13.075	100	6.0060

Table 7: SIGNAL/BACKGROUND RATIOS FOR RUNS WITH DIFFERENT MAXIMUM NEUTRON ENERGY

Sample	σ_t/σ_γ	Maximum neutron energy	Signal/Background ratio[a]		
	E_n=30 keV	(keV)	E_n=30 keV	E_n=20 keV	E_n=10 keV
^{176}Hf	21	100	7.1	3.9	2.0
^{177}Hf	7		10.0	4.5	2.9
^{178}Hf	39		5.3	2.7	1.7
^{179}Hf	12		6.4	3.2	2.0
^{180}Hf	81		3.3	1.9	1.4
^{197}Au	24		9.1	5.0	3.1
^{176}Hf		200	4.6	2.7	1.8
^{177}Hf			8.0	4.0	3.3
^{178}Hf			3.7	2.2	1.3
^{179}Hf			4.9	2.8	2.0
^{180}Hf			2.4	1.7	1.2
^{197}Au			6.7	3.8	2.4

[a]Defined as (effect+neutron scattering background)/(neutron scattering background)

with optimum signal/background ratio as indicated in Fig. 7 by vertical lines. The resulting pulse height spectra are shown in Fig. 8 for events with multiplicity >2. The threshold in sum energy is 1.6 MeV. The spectrum of the ^{176}Hf sample is the same as shown in the lower right corner of Fig. 6. The little bump above the full energy peak is clearly absent in all other samples.

Capture events are defined by summing the coincident signals from the various BaF_2 modules within a time interval of ≈10 ns. Capture cascades feeding an isomeric state do not represent the full binding energy of the captured neutron, the respective events being registered with correspondingly lower sum energies. Thanks to good energy resolution of the detector the corresponding partial cross sections can be identified by the missing sum energy, if the isomeric states are at energies above ∼250 keV. Similar to the example of the ytterbium isotopes [10] the spectra of Fig. 8 show also a significant population of

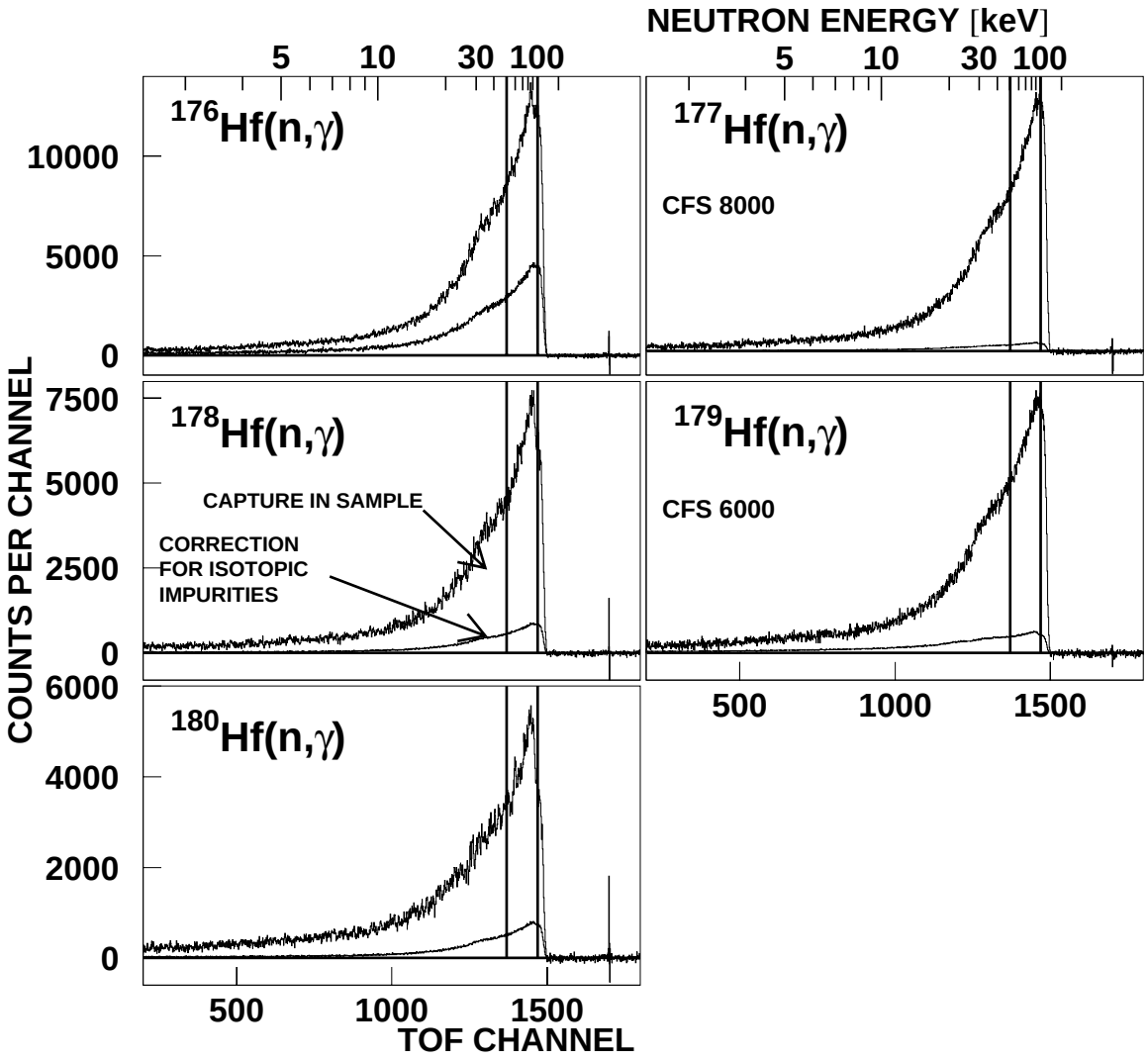

Figure 5: TOF spectra of the hafnium samples. The respective background due to isotopic impurities is shown separately.

isomeric states in some of the hafnium isotopes. Strong feeding is observed for neutron captures in ^{176}Hf and ^{179}Hf and a weak feature in case of ^{177}Hf. Most remarkably, it was found that the peak in the sum energy spectrum of neutron captures on ^{178}Hf is significantly shifted, which implies that capture to the isomer is by far the dominant reaction channel. On the other hand, feeding of isomeric states can be excluded for ^{180}Hf and for ^{197}Au. The peak in the gold spectrum is broadened and slightly shifted to lower energies but this feature has been well explained in Ref. [21] by the conversion of soft γ-transitions in the capture cascades of this high Z material.

The sum energy spectra of all isotopes are shown in Fig. 9 for various cascade multiplicities. These multiplicities correspond to the number of detector modules contributing per event, which are slightly larger than the true multiplicities because of cross talking. In the even hafnium isotopes, 22% to 38% of the capture events are observed with multiplicities $\geq$5, while the respective fraction in the odd isotopes is about 55%. The arrows in Fig. 9 indicate the range of sum energy channels that were integrated to obtain the TOF spectra of Fig. 7 for determining the cross section shapes. It is also to be noted that cascades to isomeric states exhibit a completely different multiplicity distribution

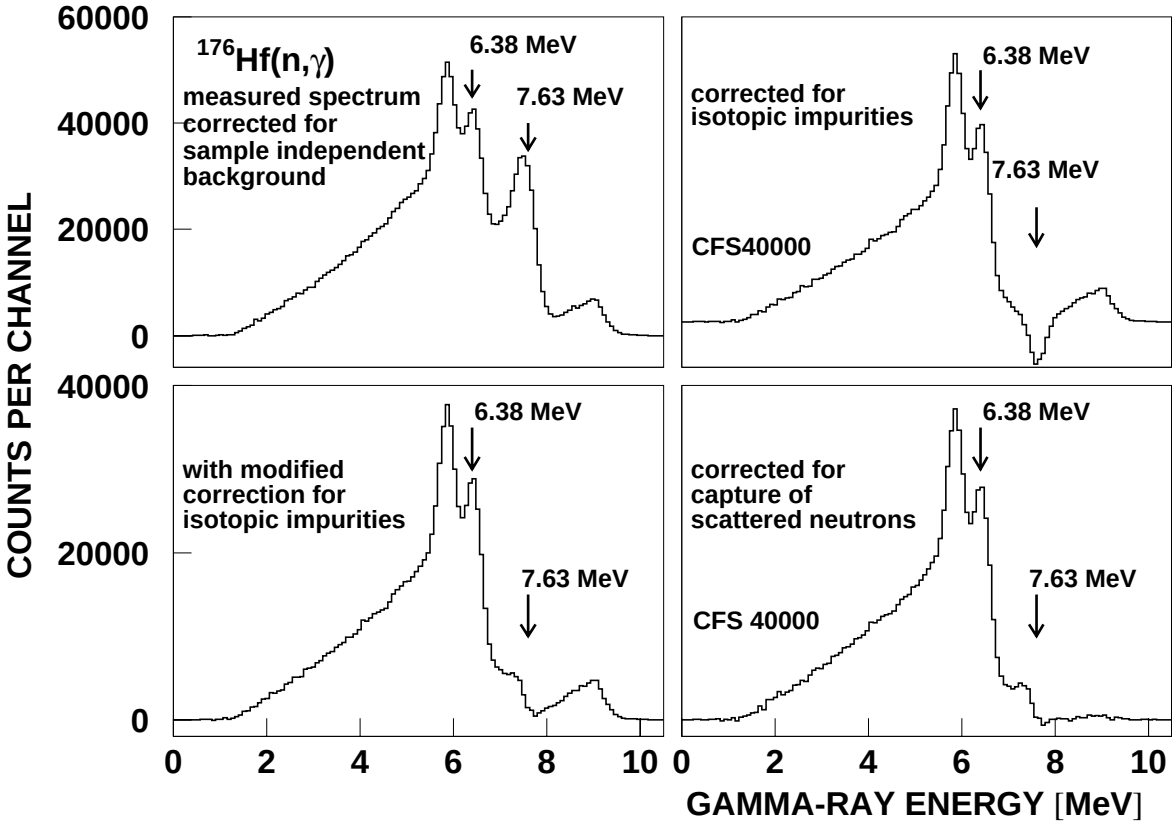

Figure 6: Sum energy spectra of the ^{176}Hf sample illustrating the various steps of data analysis. The correction of isotopic impurities according to the matrix given in Table 6 (upper right) yields an overcompensation of the ^{177}Hf impurity resulting in a dip at 7.63 MeV

compared to events leading directly to the ground state. This behavior is most pronounced for ^{176}Hf and ^{179}Hf.

The cross section ratio of isotope X relative to the gold standard is given by

$$\frac{\sigma_i(X)}{\sigma_i(Au)} = \frac{Z_i(X)}{Z_i(Au)} \frac{\Sigma Z(Au)}{\Sigma Z(X)} \frac{\Sigma E(X)}{\Sigma E(Au)} \frac{m(Au)}{m(X)} F_1 F_2. \quad (1)$$

In this expression, Z_i is the count rate of channel i in the TOF spectrum, ΣZ is the TOF rate integrated over the interval used for normalization (vertical lines in Fig. 7), ΣE is the total count rate in the sum energy spectra for all multiplicities in this TOF interval.

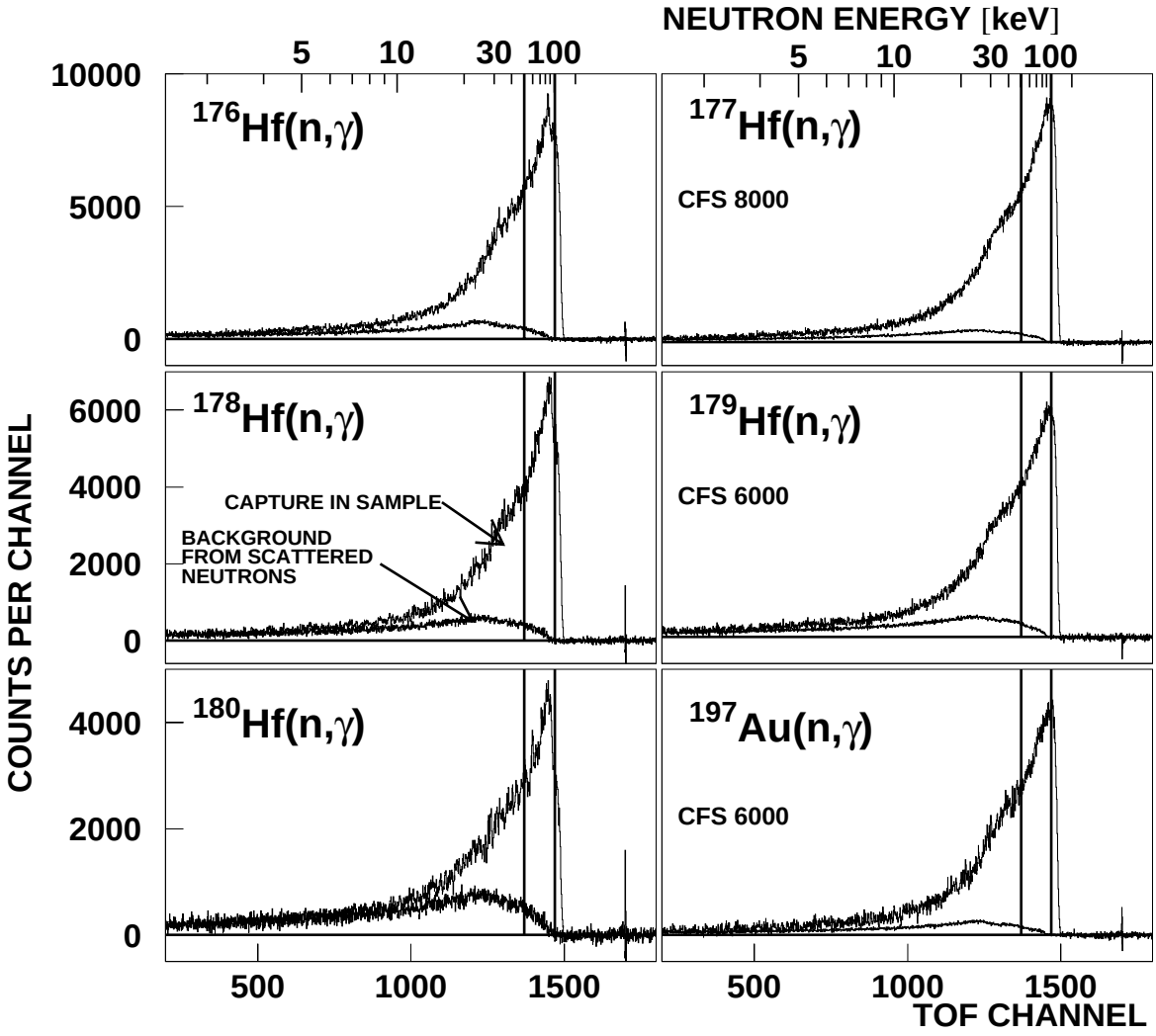

Figure 7: TOF spectra measured with the hafnium samples in run I (100 keV maximum neutron energy). The background due to sample scattered neutrons is shown separately. The region used for absolute normalization of the cross section is indicated by vertical lines.

The respective sum energy spectra are shown in Fig. 9. For all multiplicities these spectra were integrated from the threshold at 1.6 MeV beyond the binding energy, and the sum of these results, ΣE is used in Eq. 1. A full description of this procedure is given in Ref.[22]. The quantity m is the sample thickness in atoms/b.

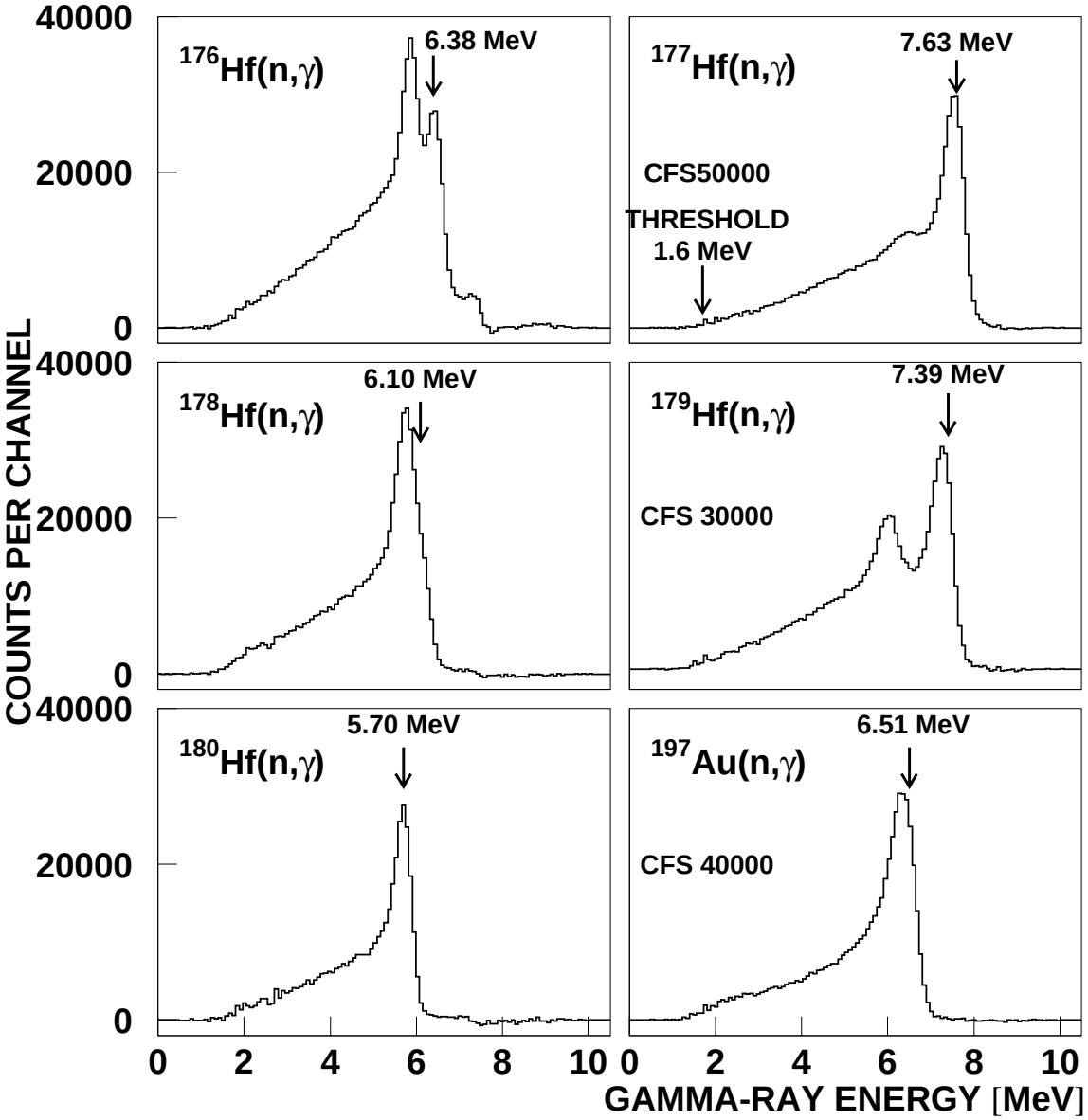

Figure 8: Sum energy spectra of events with multiplicity >2 for all isotopes measured in run I. These spectra were obtained by projection of the two–dimensional spectra in the TOF region below the maximum neutron energy as indicated by vertical lines in Fig. 7. Obviously, captures on ^{176,178,179}Hf target nuclei lead to a strong population of isomeric states.

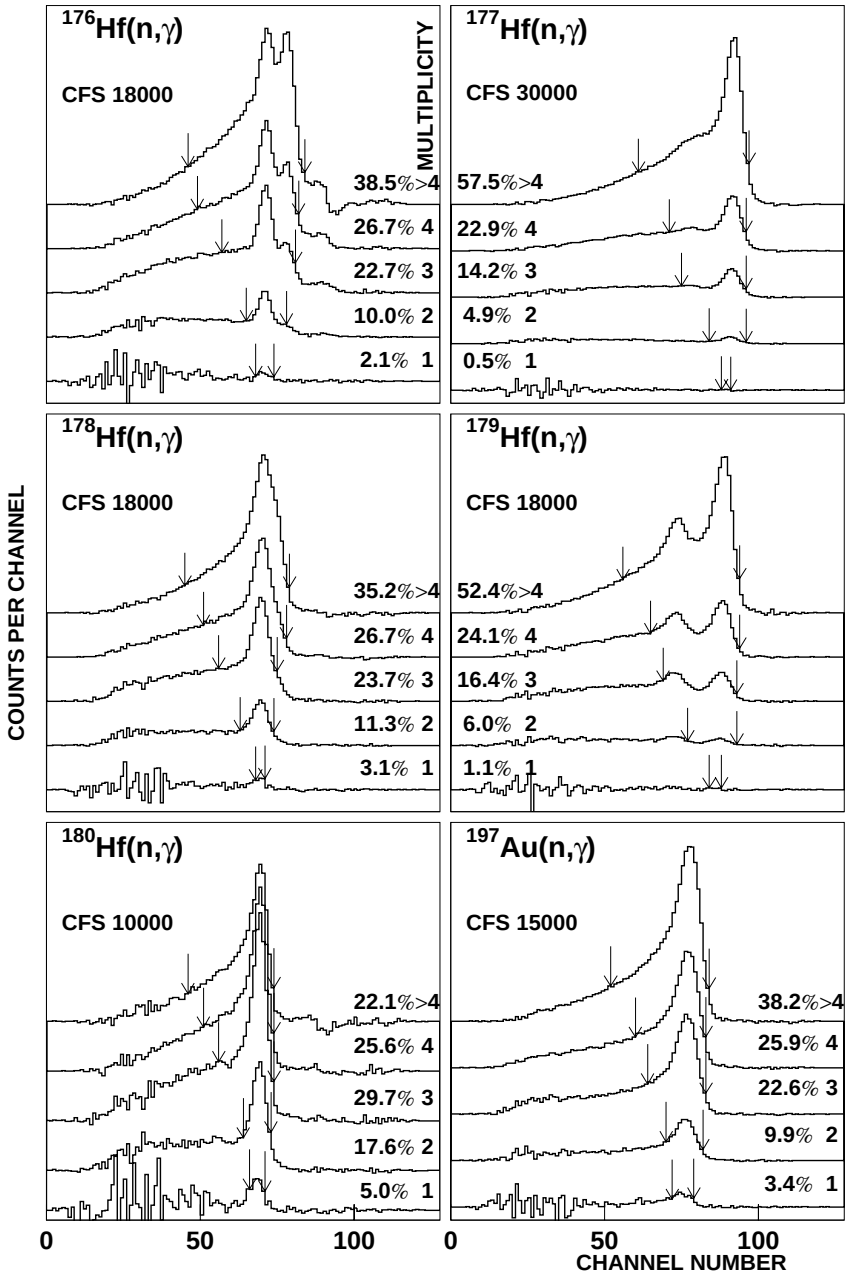

Figure 9: Sum energy spectra of all isotopes as a function of multiplicity. Integration intervals for determining the cross section shape are indicated by arrows (see TOF spectra of Fig. 7). Note that cascades to isomeric states exhibit a completely different multiplicity distribution compared to events leading directly to the ground state. This behavior is most pronounced for ^{176}Hf and ^{179}Hf.

Table 8: FRACTION OF UNDETECTED CAPTURE EVENTS, f (in %), AND THE RELATED CORRECTION FACTORS F_1.[a]

	Threshold in Sum Energy (MeV)		
	1.5	1.6	2.0
f(Au)	4.85		6.76
f(^{176}Hf)	2.42		3.92
f(^{177}Hf)	1.34		2.25
f(^{178}Hf)	3.20		5.07
f(^{179}Hf)	1.51		2.50
f(^{180}Hf)	3.95		6.15
F_1(^{176}Hf/Au)	0.975	0.974	0.970
F_1(^{177}Hf/Au)	0.964	0.962	0.954
F_1(^{178}Hf/Au)	0.983	0.983	0.982
F_1(^{179}Hf/Au)	0.966	0.964	0.956
F_1(^{180}Hf/Au)	0.991	0.991	0.993

[a] derived from capture cascades measured with the ADC system.

The factor $F_1 = [100 - f(Au)]/[100 - f(X)]$ corrects for the fraction of capture events f below the experimental threshold in sum energy, where X refers to the respective hafnium sample (Table 8), and F_2 is the ratio of the multiple scattering and self–shielding corrections.

The fraction of unobserved capture events, f, and the correction factor F_1 were calculated as described in Ref. [16]. The input for this calculation are the individual neutron capture cascades and their relative contributions to the total capture cross section as well as the detector efficiency for monoenergetic γ-rays in the energy range up to 10 MeV. As in the experiment on dysprosium isotopes [23] this information was derived directly from the experimental data recorded with the ADC system in run II. From these data, only events close to the sum energy peak (see Fig. 8) were selected, which contained the full capture γ-ray cascade. This ensemble was further reduced by restricting the analysis to the TOF region with optimum signal-to-background ratio (vertical lines in Fig. 7). The correction factors F_1 were calculated as described in Ref. [16] and are quoted in Table 8. As in all previous experiments with the 4π BaF_2 detector, F_1 was found to depend linearly on the binding energy of the captured neutron.

The capture γ-ray spectra obtained from the data taken with the ADC system are plotted in Fig. 10 in energy bins of 500 keV. The spectra of the hafnium isotopes are rather similar, except for ^{180}Hf, where the soft component is reduced while hard component is clearly enhanced.

The correction for neutron multiple scattering and self-shielding was calculated with the SESH code [17]. Apart from the pairing energies [24], most of the input parameters were taken from Ref. [25], but were slightly modified in order to reproduce the measured total and capture cross sections. The final values are listed in Table 9 together with the calculated total cross sections. The resulting correction factors, MS(X) and F_2, are compiled in Tables 10 and 11. In general, these corrections are smaller than 5% except for the even isotopes at energies below 10 keV. However, somewhat larger corrections are required for ^{180}Hf due to the larger sample mass.

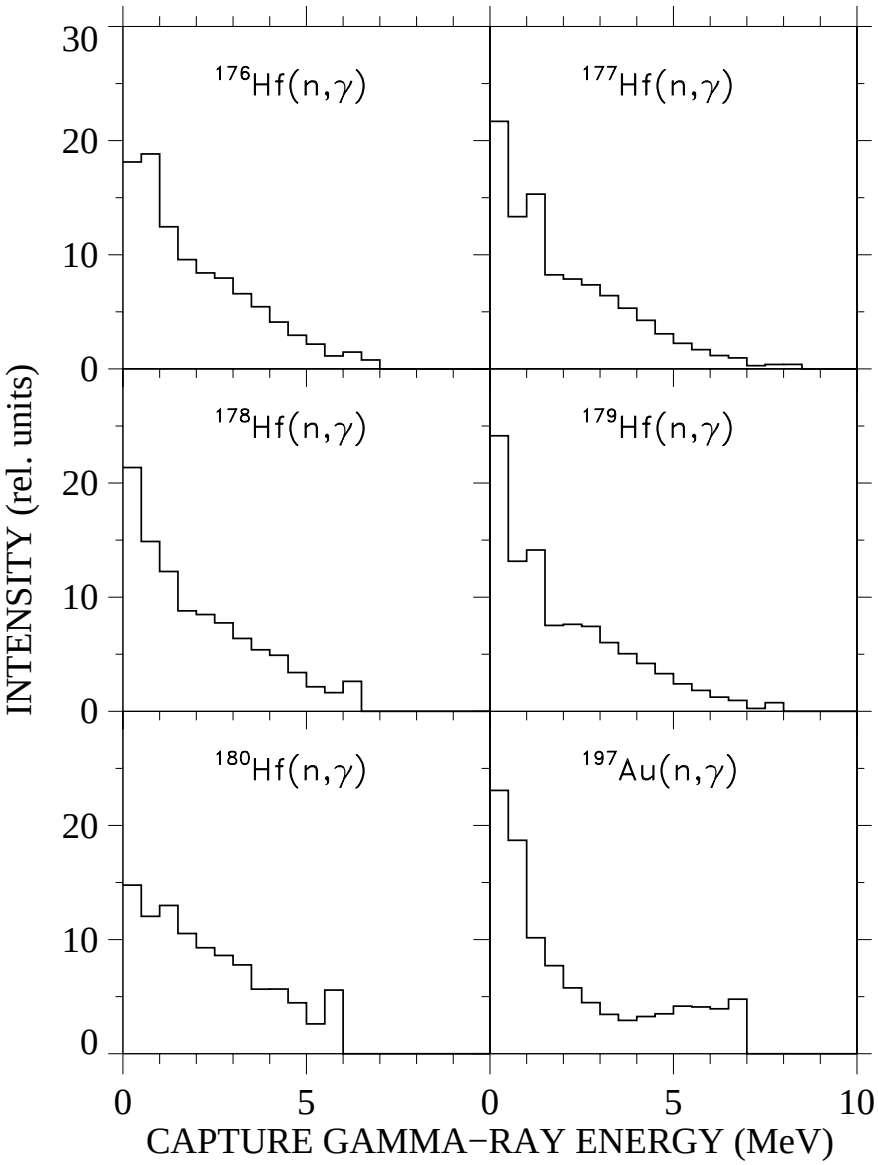

Figure 10: Capture γ-ray spectra derived from the capture cascades recorded with the ADC system. (The full resolution of 2048 channels is compressed into bins of 500 keV.)

Table 9: PARAMETERS FOR THE CALCULATION OF NEUTRON SELF–SHIELDING AND MULTIPLE SCATTERING CORRECTIONS

Parameter		^{176}Hf	^{177}Hf	^{178}Hf	^{179}Hf	^{180}Hf	^{16}O
Nucleon Number		176	177	178	179	180	16
Binding Energy (MeV)		6.383	7.626	6.100	7.388	5.696	4.144
Pairing Energy (MeV)		0.640	1.040	0.640	1.370	0.640	0.0
Effective Temperature (K)		293	293	293	293	293	293
Nuclear Spin		0	3.5	0	4.5	0	0
Average Radiation	s	0.110	0.071	0.060	0.072	0.050	0
Width (eV)	p	0.040	0.350	0.072	0.035	0.020	
	d	0.010	0.100	0.002	0.007	0.003	
Average Level	s	32.	2.4	62.	4.4	94.	0
Spacing (eV)	p[a]	10.7	1.2	20.7	2.2	31.3	
	d[a]	6.4	0.8	12.4	1.5	18.8	
Strength Function	S_0	1.8	3.2	2.2	1.7	1.7	0
(10^{-4})	S_1	1.3	0.3	0.5	0.8	0.3	
	S_2	7.0	0.4	1.7	2.1	2.6	
Nuclear Radius	s	8.2	4.5	7.5	7.7	8.0	5.5
(fm)	p	7.5	7.5	7.4	7.6	8.0	
	d	7.6	7.6	7.5	7.7	8.0	
	Calculated total cross sections						
3 keV		22.0	26.6	23.5	20.2	20.3	3.80
5 keV		18.9	21.2	19.7	17.3	17.5	3.80
10 keV		15.8	15.6	15.8	14.3	14.5	3.79
20 keV		13.5	11.7	13.0	12.2	12.3	3.77
40 keV		11.9	8.9	10.8	10.5	10.6	3.74
80 keV		10.6	6.8	9.1	9.2	9.2	3.68
160 keV		9.6	5.4	7.7	8.1	8.0	3.55
320 keV		9.2	4.6	6.6	7.3	7.2	3.31

[a]Calculated with SESH [17]

Table 10: CORRECTION FACTORS FOR NEUTRON SELF–SHIELDING AND MULTIPLE SCATTERING, MS

Energy Bin	MS					
(keV)	^{197}Au	^{176}Hf	^{177}Hf	^{178}Hf	^{179}Hf	^{180}Hf
3 – 5	0.994	0.938	1.012	0.866	1.010	0.779
5 – 7.5	1.016	0.973	1.014	0.937	1.014	0.861
7.5 – 10	1.028	0.991	1.015	0.968	1.015	0.898
10 – 12.5	1.033	1.000	1.016	0.988	1.016	0.923
12.5 –15	1.036	1.004	1.015	0.998	1.016	0.938

Table 10 (continued)

15 – 20	1.038	1.008	1.015	1.008	1.017	0.953
20 – 25	1.038	1.010	1.015	1.016	1.016	0.964
25 – 30	1.038	1.010	1.014	1.019	1.016	0.971
30 – 40	1.037	1.011	1.014	1.020	1.016	0.978
40 – 50	1.036	1.012	1.013	1.020	1.016	0.984
50 – 60	1.035	1.012	1.013	1.019	1.015	0.988
60 – 80	1.034	1.012	1.013	1.018	1.015	0.993
80 – 100	1.032	1.012	1.012	1.018	1.015	0.998
100 – 120	1.031	1.013	1.012	1.019	1.015	1.003
120 – 150	1.030	1.013	1.011	1.019	1.015	1.007
150 – 175	1.029	1.013	1.011	1.019	1.014	1.009
175 – 200	1.028	1.014	1.011	1.020	1.014	1.011
200 – 225	1.027	1.015	1.010	1.020	1.014	1.013
Uncertainty (%)	0.3	0.2	0.1	0.3	0.2	0.6

Table 11: CORRECTION FACTORS FOR THE CROSS SECTION RATIOS, F_2 = MS(Au)/MS(X)

Energy Bin	F_2				
(keV)	^{176}Hf/Au	^{177}Hf/Au	^{178}Hf/Au	^{179}Hf/Au	^{180}Hf/Au
3 – 5	1.060	0.982	1.148	0.984	1.276
5 – 7.5	1.044	1.002	1.084	1.002	1.180
7.5– 10	1.037	1.013	1.062	1.013	1.145
10 – 12.5	1.033	1.017	1.046	1.017	1.119
12.5 – 15	1.032	1.021	1.038	1.020	1.105
15 – 20	1.030	1.023	1.030	1.021	1.089
20 – 25	1.028	1.023	1.022	1.022	1.077
25 – 30	1.028	1.024	1.019	1.022	1.069
30 – 40	1.026	1.023	1.017	1.021	1.060
40 – 50	1.024	1.023	1.016	1.020	1.053
50 – 60	1.023	1.022	1.016	1.020	1.048
60 – 80	1.022	1.021	1.016	1.019	1.041
80 – 100	1.020	1.020	1.014	1.017	1.034
100 – 120	1.018	1.019	1.012	1.016	1.028
120 – 150	1.017	1.019	1.011	1.015	1.023
150 – 175	1.016	1.018	1.010	1.015	1.020
175 – 200	1.014	1.017	1.008	1.014	1.017
200 – 225	1.012	1.017	1.007	1.013	1.014
Uncertainty (%)	0.4	0.3	0.4	0.4	0.7

4 ISOMERIC RATIOS AND GEANT SIMULATIONS

For neutron captures in ^{177,178,179}Hf the significant population of isomeric states can be ascribed to three isomers at 1147 keV, 375 keV, and 1374 keV in the respective compound nuclei [26]. By comparison of these cases it is surprising to see that neutron capture in ^{178}Hf seems to feed exclusively the isomeric state in ^{179}Hf. The case of neutron captures in ^{176}Hf is particularly interesting, since the observed structure of the leading peak in the sum energy spectrum of Fig. 8 is clearly indicating an isomer in ^{177}Hf, whereas there is no such level known with an energy around 500 keV and a half life longer than 10 ns.

Two attempts have been made to separate the components of captures to the ground and the isomeric states, an empirical approach by fitting the measured spectra with appropriate line shapes, and a theoretical description constructing the neutron capture cascades by using all available information on the involved level schemes. These theoretical cascades, which provide already a theoretical estimate of the isomeric ratio, were then used as input for a complete GEANT [27] simulation of the experiment. This technique has successfully been used to quantitatively reproduce the measured sum energy spectra and multiplicity distributions [28] [21].

4.1 Empirical determination of isomeric ratios

In Fig. 8 the population of isomers is clearly observed for neutron captures in ^{176,177,178,179}Hf. In order to determine the isomeric ratio IR, which is defined as the ratio of the partial capture to the isomeric state and the total capture cross section, the respective partial cross sections have been separated. For this purpose sum energy spectra of about 20 isotopes, that have been measured with the Karlsruhe 4π BaF_2 detector previously, were generated from capture events in the neutron energy range from 50 keV to 100 keV. These spectra, none of which was affected by isomeric states, were fitted by the superposition of a gaussian for the sum energy peak and a truncated polynomial for the low energy tail as described in Ref. [8]. As a result, a consistent systematics could be established for the fit parameters, characterizing a wide range of binding energies from 4.78 MeV (^{232}Th) to 8.54 MeV (^{155}Gd).

Based on this parameter systematics, the two components in the spectra of Fig. 8 corresponding to captures feeding the isomer and groundstate in the hafnium isotopes 177 to 180, could be constrained with respect to their spectral shape. In each case, the intensity ratio of sum energy peaks and low energy tail was fixed by the systematics, leaving only the height and width of the sum energy peak as adjustable parameters. This procedure was tested by varying the individual parameters in a range consistent with the spread of the systematics with the result that the derived isomeric ratios were fairly stable.

The three experimental runs were analyzed individually, yielding consistent isomeric ratios for all target isotopes. The fits to the spectra of run I are presented in Figs. 11 and 12 with the isomer energies indicated in the legend. Direct assignment of these energies to known isomers could be made for ^{178}Hf^m, ^{179}Hf^m, and ^{180}Hf^m whereas the energy of the previously unknown isomer in ^{177}Hf had to be postulated. The respective isomeric ratios, IR =partial cross section to isomer/total cross section, are summarized in Table 12.

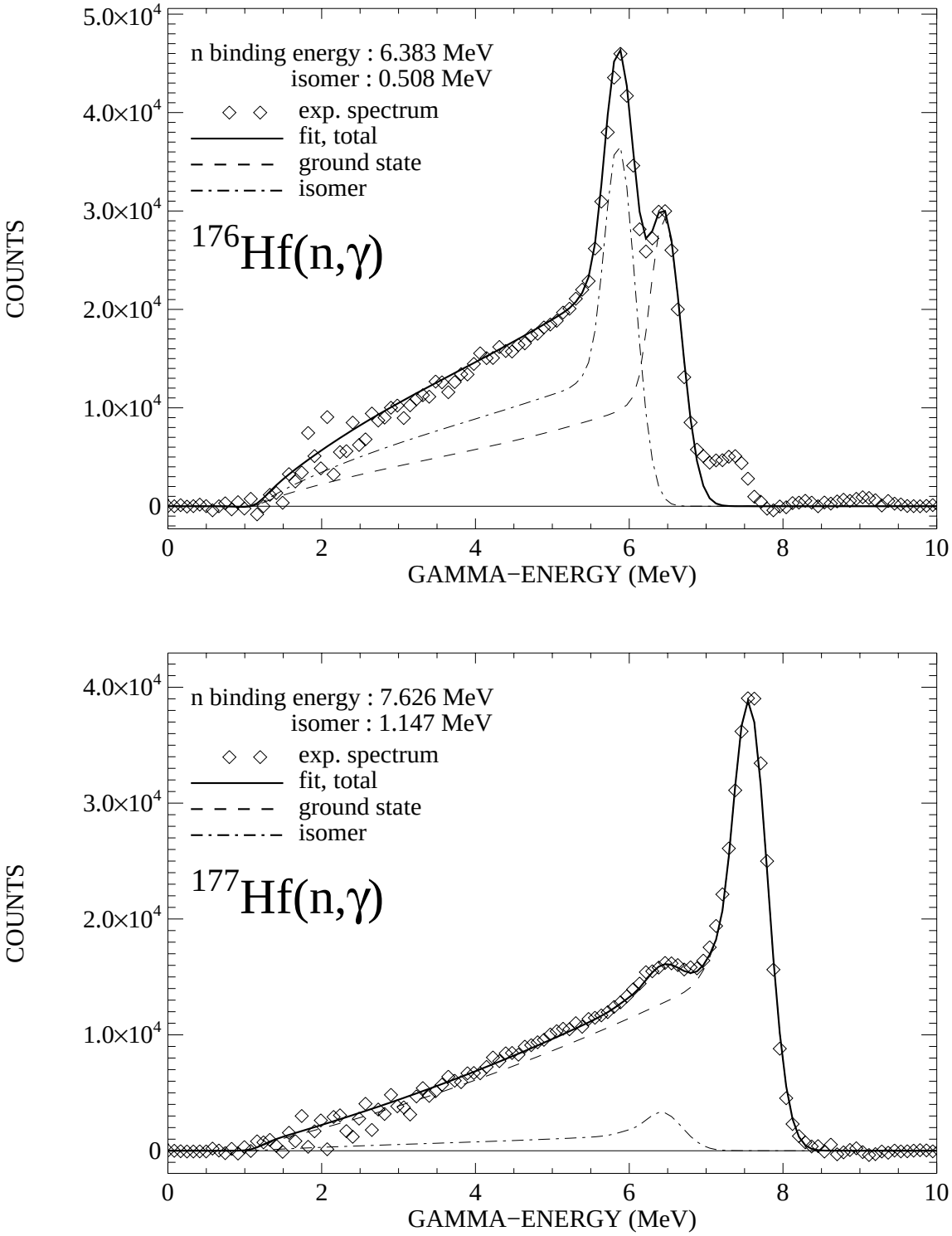

Figure 11: Fit to the experimental sum energy spectra for neutron capture in ^{176}Hf and ^{177}Hf given in Fig 9. The two components of capture to ground state and isomer are shown separately. The isomer energies given in the legend were used in the fit. The isomer in ^{177}Hf around 508 keV was unknown before.

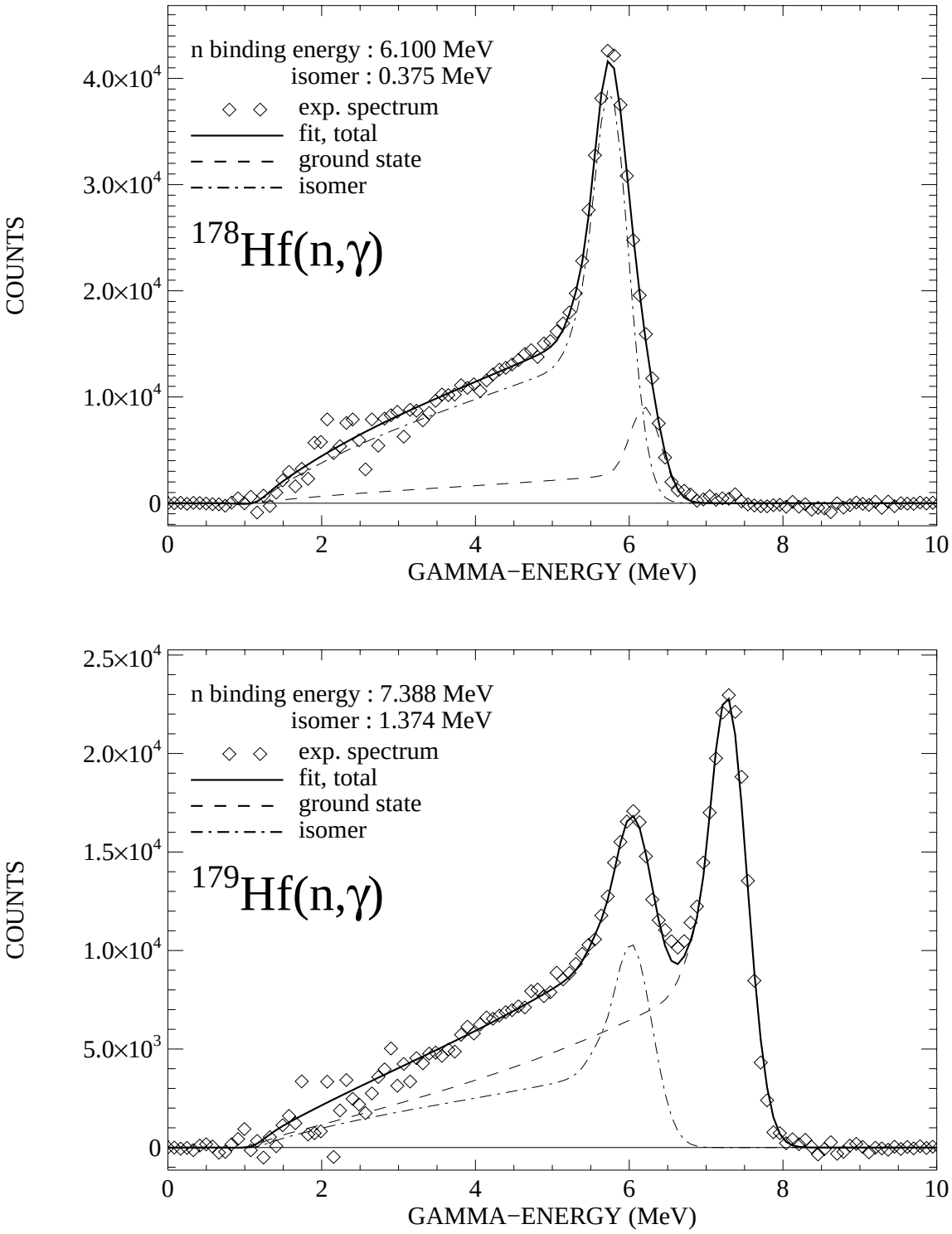

Figure 12: The same as Figure 11 but for neutron capture in ^{178}Hf and ^{179}Hf.

Table 12: ISOMERIC RATIOS FOR NEUTRON CAPTURES IN VARIOUS HAFNIUM ISOTOPES

Isomeric ratio	Target nucleus			
	^{176}Hf	^{177}Hf	^{178}Hf	^{179}Hf
E_n = 75 keV, empirical determination	0.51±0.02	0.08±0.01	0.81±0.02	0.28±0.02
E_n = 75 keV, calculated with CASINO	0.05	0.01	0.58	0.08
thermal neutrons [25]	–	0.003	0.63	0.01

4.2 Calculation of neutron capture cascades

For an independent determination of the isomeric ratio γ-ray cascades from neutron capture reactions on the investigated hafnium isotopes were calculated using the CASINO [29] version of the Monte Carlo code DICEBOX [30] which is well suited for the keV neutron energy range. For the GEANT simulations described below, the proper treatment of the probability for emission of conversion electrons is an important feature of this code. Each of the simulations was carried out with a set of about 10000 neutron capture cascades. Within the individual cascades each step is marked to distinguish γ-ray transitions from transitions due to conversion electrons.

Neutron captures in ^{176}Hf are clearly populating a yet unknown isomer at about 508 keV. Since no isomeric state is reported in ^{177}Hf [31] near this energy, the isomer was assumed to correspond to an uncertain level at 608 keV. Neutron capture in even-even nuclei starts at a state with $J^{\pi}=0^{+}$. According to our cascade model, only an isomer with $J^{\pi}_{isomer} = 1/2^{+}$ can be weakly populated via s- and p-wave capture, although 10 times weaker than observed (Table 12).

In case of ^{180}Hf an isomeric state is reported at 1374 keV with $J^{\pi} = 3^{-}$ and $t_{1/2}$ = 570 ns [32]. However, the calculated population is far too to account for the measured isomeric ratio. This problem seem to suggest the existence of an additional, yet unknown isomeric state in ^{180}Hf at about 1490 keV.

The isomers in the other two isotopes, ^{178}Hf and ^{179}Hf, could be well reproduced as shown in Table 12.

In contrast to the other cases, the experimental sum energy spectrum of neutron capture in ^{180}Hf exhibits no indication for an isomer in ^{181}Hf, in agreement with the reported level scheme [33].

Although the general trend seems to be qualitatively followed, the isomeric ratios are systematically underestimated in the CASINO calculations. In fact, the calculated values are much closer to the values measured for thermal neutron energies [25] (Table 12), reflecting deficiencies concerning the discrete level schemes and the level densities at higher excitation.

4.3 GEANT simulations

A significant step in the interpretation of the spectra measured with the Karlsruhe 4π BaF_2 detector was recently achieved by complete, detailed GEANT [27] simulations of the experimental setup [28]. For this purpose the GEANT data base was improved with respect to low energy neutron experiments by implementation of the most recent neutron and gamma cross sections. The complex geometry of the Karlsruhe 4π BaF_2 detector was modeled for all 41 crystals including reflectors, photomultipliers, and all structural materials. The efficiency for γ-rays originating from a sample in the center of the detector was then calculated including the effect of γ-ray self absorption in the sample and in the sample can. Internal conversion of γ-transitions was considered as well, which is important for obtaining the proper shape of the sum energy spectra, since conversion electrons are easily absorbed and do not contribute to the scintillation signal of the barium fluoride crystals. In this way, the spectra were calculated for each single crystal and the effect of cross talking could be evaluated in detail. The energy resolution of the individual crystals were normalized by means of actual spectra measured with calibration sources.

Table 13: FRACTION OF UNDETECTED CAPTURE EVENTS, f (in %), AND THE RELATED CORRECTION FACTORS F_1.[a]

	Threshold in Sum Energy (MeV)		
	1.5	1.6	2.0
f(Au)	4.19		6.68
f(^{176}Hf)	2.41		4.76
f(^{177}Hf)	1.10		2.20
f(^{178}Hf)	3.62		6.79
f(^{179}Hf)	1.20		2.50
f(^{180}Hf)	4.60		8.38
F_1(^{176}Hf/Au)	0.982	0.982	0.980
F_1(^{177}Hf/Au)	0.969	0.966	0.954
F_1(^{178}Hf/Au)	0.994	0.995	1.001
F_1(^{179}Hf/Au)	0.970	0.967	0.957
F_1(^{180}Hf/Au)	1.004	1.007	1.019

[a] derived from the GEANT simulations

The calculated neutron capture cascades were also used to determine the response of the 4π BaF_2 detector by means of the GEANT simulations. For each cascade the γ-rays or electrons of the individual transitions were started in random directions at a common point inside the sample. The starting points were isotropically distributed over the volume of the sample and the deposited energy in the various detector modules was

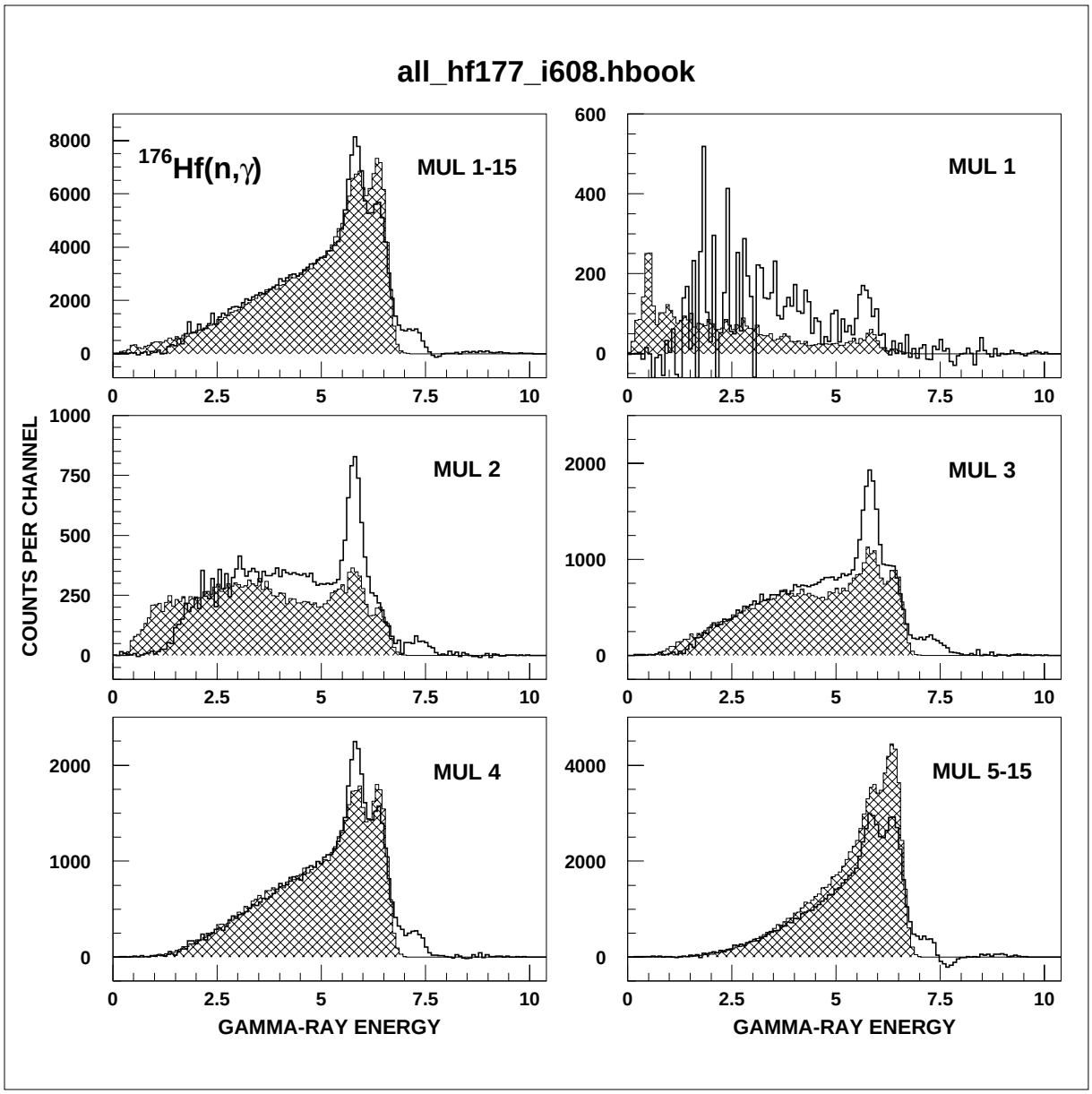

Figure 13: Simulated sum energy spectra for different multiplicities for neutron capture in ^{176}Hf (hatched areas) compared to the experimental spectra of Fig 9 (histograms).

followed down to the experimental threshold of ≈50 keV.

Since each capture cascade was simulated separately, the spectra of the individual crystals and also the sum energy spectra could be stored as a function of multiplicity.As defined in Section 3, the multiplicity of an event is given by the total number of crystals, which registered an energy signal above 50 keV. The total recorded energy (sum energy) of this cascade was then stored in the respective multiplicity spectrum. Events were found with multiplicities between 1 and 15, but with strongly decreasing probability above multiplicities of about 6. These simulated spectra are compared with the experimental results of Fig 9 in Figs. 13 to 17. In the upper left corner of Figs. 13 to 17 the total

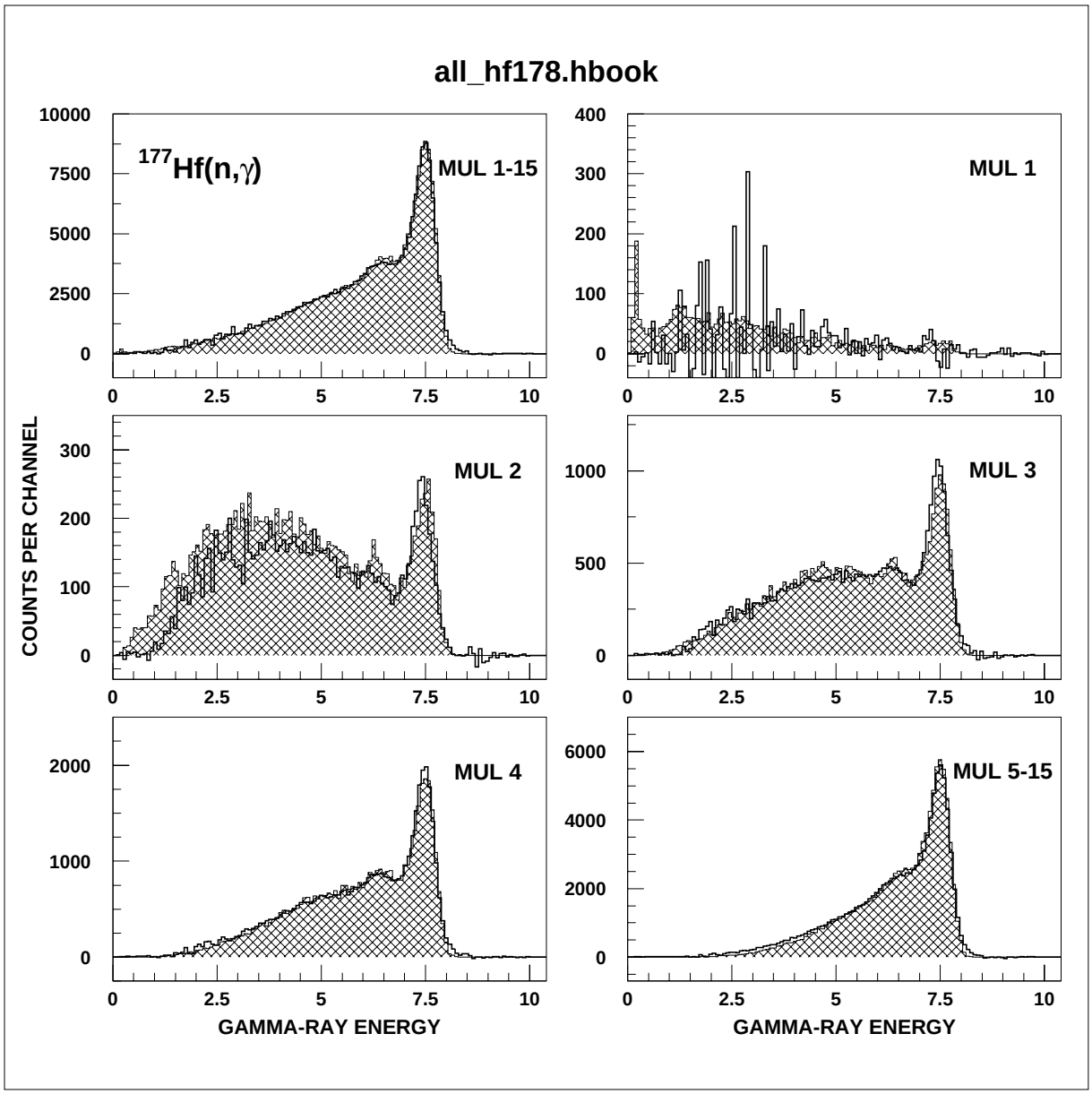

Figure 14: Simulated sum energy spectra for different multiplicities for neutron capture in ^{177}Hf (hatched areas) compared to the experimental spectra of Fig 9 (histograms).

sum of all multiplicities is given as in Fig. 8, whereas the other five spectra correspond to the data shown in Fig. 9. It is important to note that the simulated spectra are only normalized via the total number of measured events.

The comparison of the measured and simulated spectra show surprisingly good agreement with respect to the sum energy peak at the binding energy of the captured neutron as well as for the tail towards lower energies, although this tail shows large statistical fluctuations in the experimental spectra with multiplicities 1 and 2 because of the large backgrounds in this region. Nevertheless, the multiplicity distribution is well reproduced for all hafnium isotopes.

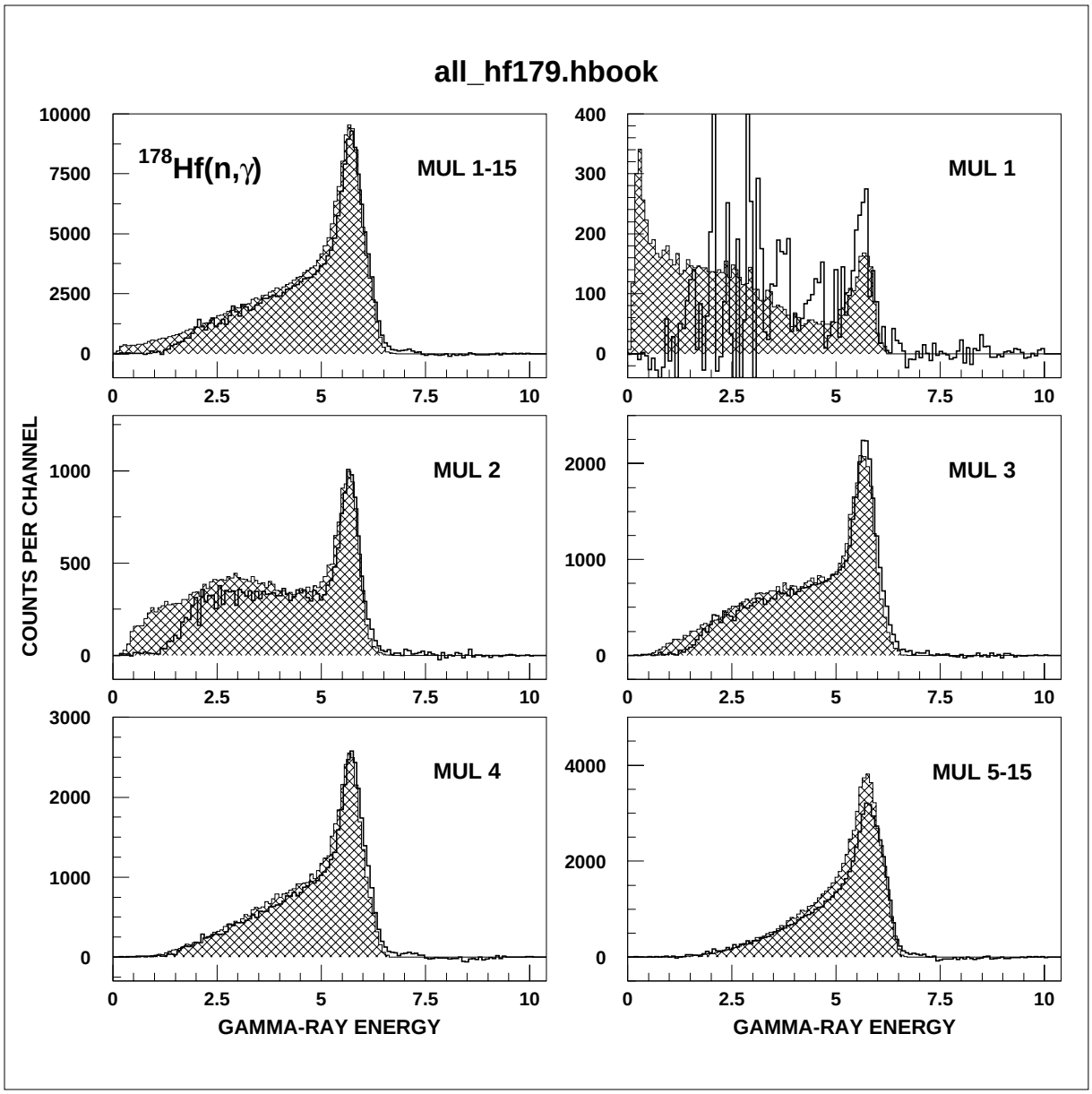

Figure 15: Simulated sum energy spectra for different multiplicities for neutron capture in ^{178}Hf (hatched areas) compared to the experimental spectra of Fig 9 (histograms).

However there are severe discrepancies correlated with the population of isomeric states. In case of ^{176}Hf it is obvious that the simulation does not account for the observed population of the isomeric state in ^{177}Hf. This discrepancy could not be solved, even if the parity of the postulated isomeric state was tuned in order to obtain the highest possible population. A better description of the experimental data would require the questionable assumption of two additional $J^{\pi}=1/2^{+}$ isomers at 615 and 618 keV.

Similarly, neutron capture in ^{179}Hf exhibits severe discrepancies concerning the feeding of the 1374 keV isomer in ^{180}Hf. Even if the spin of this isomer was artificially changed from 3 to 4, i.e. closer to the target spin of 9/2, this situation persisted. Again, the only

solution within the present approach seemed to require two additional $J^{\pi}=5^{-}$ isomers at 1374 and 1376 keV. The well established 8^{-} isomer at 1141 keV, however, was correctly described to be very weakly populated, in agreement with the experimental result of Ref. [34].

In the remaining cases, i.e. for neutron capture in ^{177}Hf and ^{178}Hf, the calculated capture cascades led to good agreement between simulation and experiment, accounting even for the surprising finding that neutron capture in ^{178}Hf leads nearly exclusively to the isomer. For neutron capture in ^{180}Hf, which is not affected by isomeric states, the experimental spectra are also well described by the simulations.

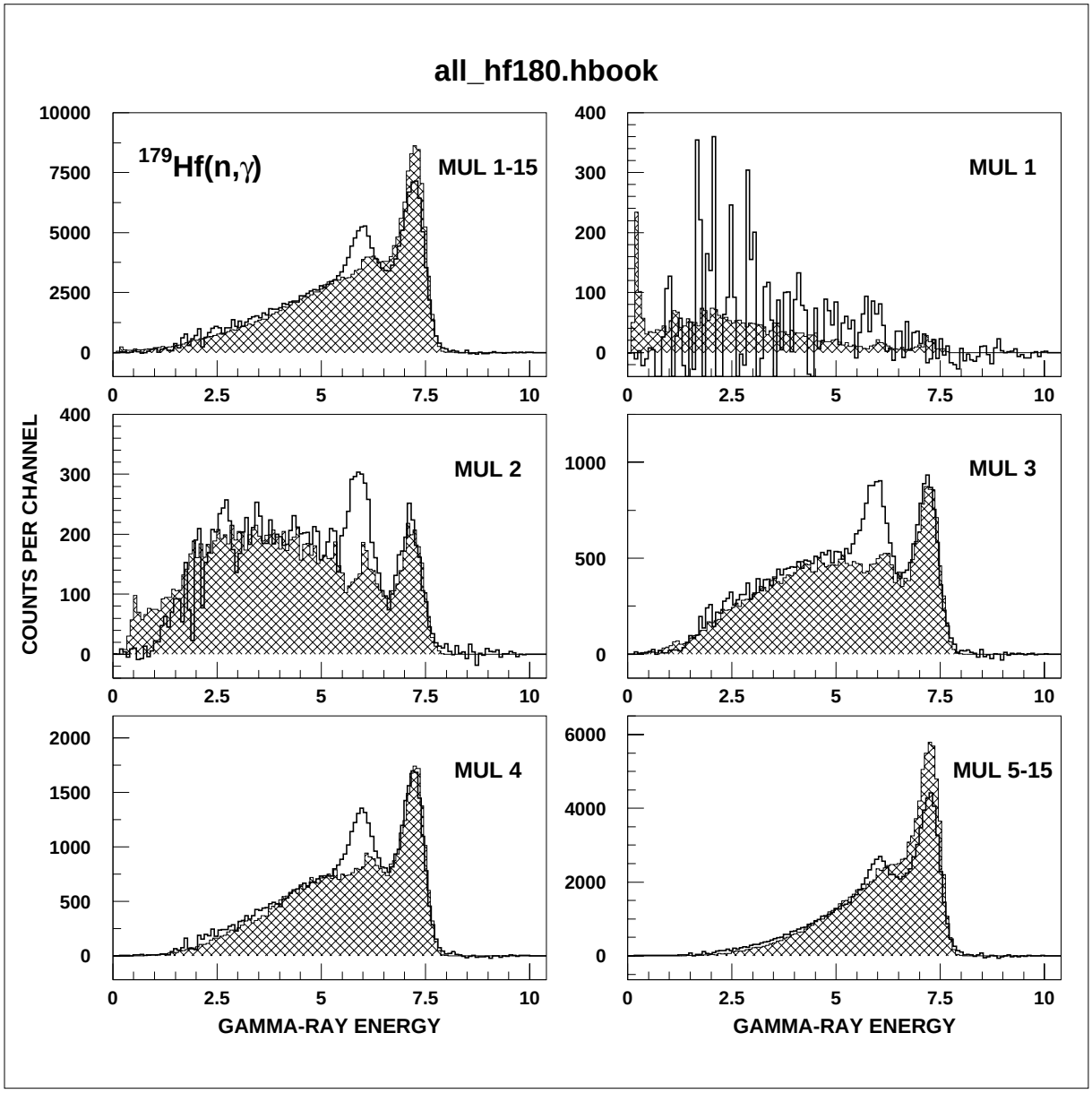

Figure 16: Simulated sum energy spectra for different multiplicities for neutron capture in ^{179}Hf (hatched areas) compared to the experimental spectra of Fig 9 (histograms).

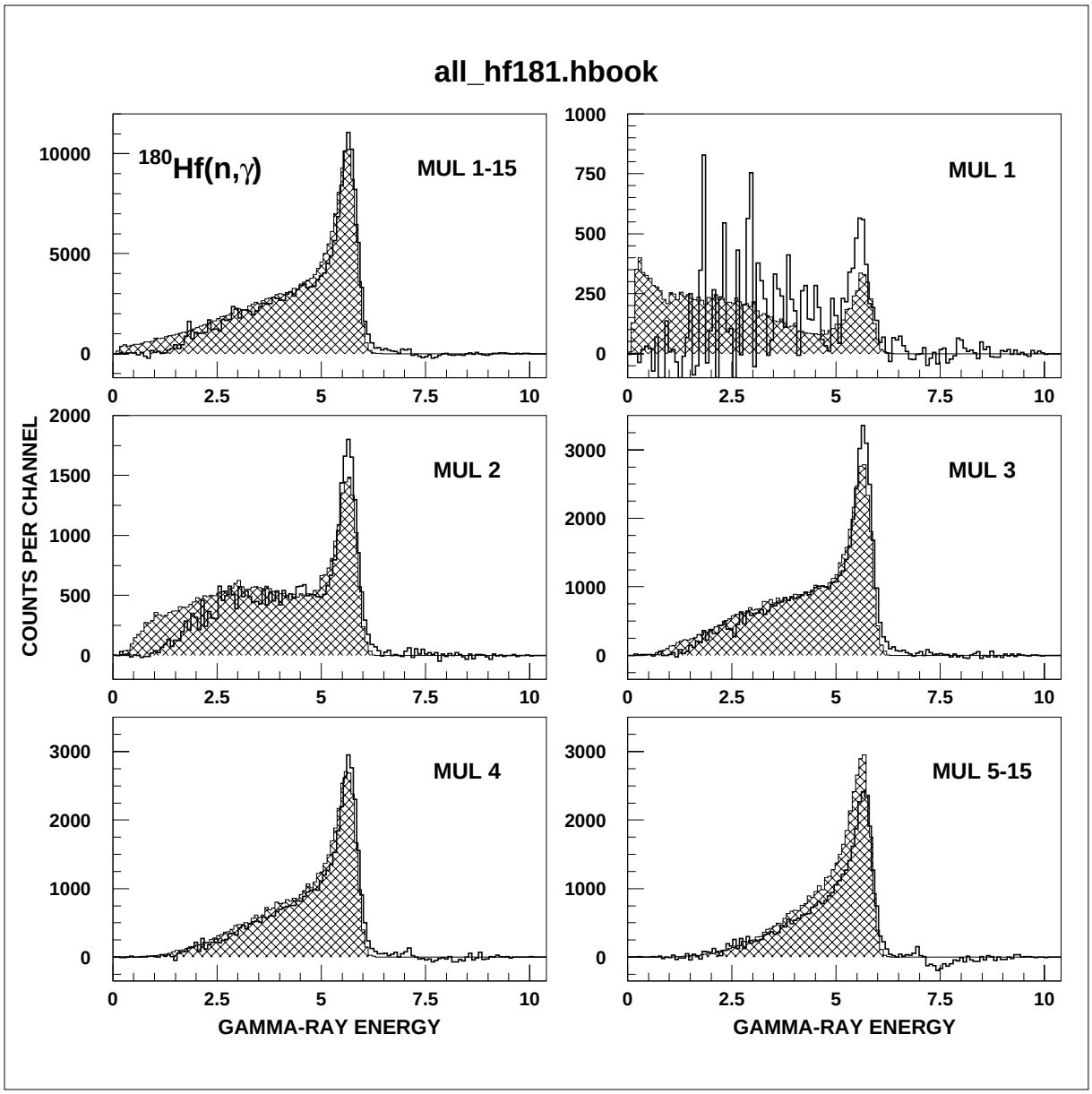

Figure 17: Simulated sum energy spectra for different multiplicities for neutron capture in ^{180}Hf (hatched areas) compared to the experimental spectra of Fig 9 (histograms).

Apart from the attempt to model the isomeric ratios, the main purpose of the simulations was to provide an independent check of the correction for the fraction of capture events, which escaped detection. This check is important since the overall systematic uncertainty of the measured cross sections is dominated by this correction. The respective spectrum fractions f below sum energy thresholds of 1.5 and 2 MeV were deduced from the simulated spectra in the upper left corner of Figs. 13 to 17 and are listed in Table 13 together with the corresponding correction factors F_1 for the cross section ratio relative to the gold standard. At the actual experimental threshold energies of 1.5 and 1.6 MeV the simulated results for F_1 agree with the values obtained from the experimentally measured

cascades (Table 8) within 0.8% on average. This agreement between the independently determined corrections confirms the uncertainties assigned to this correction in the past.

5 DIFFERENTIAL NEUTRON CAPTURE CROSS SECTIONS

The neutron capture cross section ratios of the investigated Hf isotopes, and of ^{197}Au are listed for all runs and for the two evaluation methods discussed in Sec. 3 in Tables 14 to 18 together with the respective statistical uncertainties. The last column in each table contains the weighted average, the weight being determined by the inverse of the squared statistical uncertainties. Since the cross section ratios depend weakly on energy, the averages for the energy interval from 30 to 80 keV are also included for a better comparison of the individual results. The data are free of systematic differences with respect to different runs or evaluations. On average, all observed differences are well within the quoted statistical uncertainties, except for ^{176}Hf, where differences of 2% appear between evaluation 1 and 2. This seems to reflect the problems in calculating the large correction for isotopic impurities for this sample (see Sec. 3).

As in the previous measurements with the 4π BaF_2 detector [13, 14, 35], the final cross section ratios were adopted from evaluation 2. The respective mean values are compiled in Table 19 together with the statistical, systematic, and total uncertainties. The energy bins are sufficiently fine to avoid systematic uncertainties in the calculation of the Maxwellian averaged cross sections (Sec. 7). In the energy bins between 15 and 100 keV statistical uncertainties of less than 1.0% could be obtained for nearly all investigated cross sections. The systematic uncertainties range between 0.7 and 1.7%.

The experimental ratios were converted into absolute cross sections using the gold data of Macklin [36] after normalization by a factor of 0.989 to the absolute value of Ratynski and Käppeler [37] (Table 20). The uncertainties of the resulting values can be obtained by adding the 1.5% uncertainty of the reference cross section to the uncertainties of the respective cross section ratios.

The present results are compared to previous data of Beer *et al.* [4, 11] and Bokhovko *et al.* [12] in Figs. 18 to 20. The uncertainties of 3% - 6% quoted for the older values, which seem to be rather optimistic in view of the discrepancies among the ^{177}Hf and ^{179}Hf data, could be significantly improved. For ^{177}Hf, ^{178}Hf, and ^{179}Hf the present results are very close to the average of the previous experiments, while the new data are systematically lower by ∼10% for ^{180}Hf. For the important *s*-only isotope ^{176}Hf, the new cross section is systematically larger by ∼40%. A reason for this discrepancy may well be due to the correction for isotopic impurities. While the samples in the previous experiments showed similar enrichment in ^{176}Hf, the respective corrections were much more difficult because of the lower γ-ray efficiency and the missing sum energy information inherent to the detection methods used.

Table 14: $\sigma(^{176}\mathrm{Hf})/\sigma(^{197}\mathrm{Au})$ AND STATISTICAL UNCERTAINTIES (in %)

Energy Bin (keV)	Run I		Run II		Run III		Average	
evaluation 1								
3 – 5	1.1478	7.1	1.0292	9.7	1.1024	14.	1.1060	5.3
5 – 7.5	0.9714	4.0	1.0361	5.6	1.1142	8.0	1.0106	3.0
7.5 – 10	1.1231	3.5	0.9425	4.3	1.1036	6.8	1.0588	2.5
10 – 12.5	1.0827	2.6	1.0218	3.2	1.0813	5.3	1.0615	1.9
12.5 – 15	1.0459	2.3	0.9813	2.9	0.9698	5.0	1.0152	1.7
15 – 20	1.1204	1.4	1.0663	1.8	1.0689	2.9	1.0965	1.0
20 – 25	1.1850	1.2	1.1357	1.5	1.1152	2.4	1.1590	0.9
25 – 30	1.1865	1.0	1.1339	1.3	1.1042	1.9	1.1579	0.7
30 – 40	1.1928	0.8	1.1543	1.0	1.2187	1.3	1.1867	0.6
40 – 50	1.2445	0.8	1.2001	1.1	1.2391	1.3	1.2312	0.6
50 – 60	1.2655	0.7	1.2163	1.0	1.2676	1.3	1.2526	0.5
60 – 80	1.2782	0.6	1.2283	0.9	1.2598	1.0	1.2618	0.5
80 – 100	1.2549	0.6	1.2200	0.9	1.2538	1.0	1.2462	0.5
100 – 120	1.1058	0.7	1.0382	1.1	1.1037	1.0	1.0889	0.5
120 – 150	–	–	–	–	1.0018	0.9	1.0018	0.9
150 – 175	–	–	–	–	0.9216	1.0	0.9216	1.0
175 – 200	–	–	–	–	0.9117	1.2	0.9117	1.2
200 – 225	–	–	–	–	0.8971	1.6	0.8971	1.6
30 – 80	1.2453	0.5	1.1998	0.8	1.2463	0.7	1.2331	0.4
evaluation 2								
3 – 5	0.8586	5.8	0.7982	8.2	0.7762	13.	0.8308	4.4
5 – 7.5	0.8612	3.3	0.9063	4.5	0.8976	6.8	0.8797	2.5
7.5 – 10	0.9640	2.9	0.8956	3.4	0.9355	5.5	0.9359	2.0
10 – 12.5	0.9965	2.1	0.9468	2.6	0.9732	4.4	0.9765	1.5
12.5 – 15	0.9694	1.9	0.9422	2.3	0.9341	4.2	0.9555	1.4
15 – 20	1.0578	1.2	1.0297	1.5	1.0130	2.4	1.0427	0.9
20 – 25	1.1352	1.0	1.0921	1.2	1.0847	2.0	1.1134	0.7
25 – 30	1.1368	0.8	1.0957	1.1	1.0949	1.6	1.1172	0.6
30 – 40	1.1709	0.6	1.1306	0.8	1.1961	1.1	1.1629	0.5
40 – 50	1.2140	0.6	1.1743	0.9	1.2073	1.1	1.2009	0.5
50 – 60	1.2369	0.6	1.1926	0.8	1.2572	1.1	1.2273	0.5
60 – 80	1.2557	0.5	1.2124	0.7	1.2388	0.9	1.2403	0.4
80 – 100	1.2237	0.5	1.1958	0.7	1.2325	0.9	1.2178	0.4
100 – 120	1.0810	0.6	1.0104	0.9	1.0920	0.9	1.0649	0.4
120 – 150	–	–	–	–	0.9878	0.8	0.9878	0.8
150 – 175	–	–	–	–	0.9070	1.0	0.9070	1.0
175 – 200	–	–	–	–	0.8934	1.1	0.8934	1.1
200 – 225	–	–	–	–	0.8847	1.5	0.8847	1.5
30 – 80	1.2194	0.4	1.1775	0.6	1.2249	0.6	1.2079	0.3

Table 15: $\sigma(^{177}\mathrm{Hf})/\sigma(^{197}\mathrm{Au})$ AND STATISTICAL UNCERTAINTIES (in %)

Energy Bin (keV)	Run I		Run II		Run III		Average	
evaluation 1								
3 – 5	2.7370	7.3	2.0984	11.	2.1429	16.	2.4880	5.7
5 – 7.5	2.2600	4.3	2.3849	6.0	2.3411	9.3	2.3074	3.3
7.5 – 10	2.5203	3.8	2.3551	4.4	2.4726	7.6	2.4531	2.7
10 – 12.5	2.3025	2.9	2.3863	3.4	2.4914	5.9	2.3567	2.1
12.5 – 15	2.4686	2.5	2.4670	3.0	2.5909	5.1	2.4829	1.8
15 – 20	2.6121	1.5	2.6208	1.9	2.6690	3.0	2.6223	1.1
20 – 25	2.8938	1.2	2.8489	1.6	2.8121	2.4	2.8676	0.9
25 – 30	2.7821	1.0	2.7721	1.3	2.7538	2.0	2.7748	0.8
30 – 40	2.7876	0.8	2.7536	1.1	2.8035	1.3	2.7806	0.6
40 – 50	2.8254	0.8	2.8328	1.1	2.8405	1.4	2.8302	0.6
50 – 60	2.8075	0.8	2.8406	1.1	2.8057	1.3	2.8164	0.6
60 – 80	2.8651	0.7	2.8842	0.9	2.8178	1.0	2.8597	0.5
80 – 100	2.9695	0.7	2.9954	0.9	2.9556	1.0	2.9725	0.5
100 – 120	2.9043	0.7	2.9142	1.0	2.8877	1.0	2.9022	0.5
120 – 150	–	–	–	–	2.6764	0.9	2.6764	0.9
150 – 175	–	–	–	–	2.5784	1.0	2.5784	1.0
175 – 200	–	–	–	–	2.5842	1.1	2.5842	1.1
200 – 225	–	–	–	–	2.5564	1.6	2.5564	1.6
30 – 80	2.8214	0.5	2.8278	0.8	2.8169	0.6	2.8217	0.4
evaluation 2								
3 – 5	2.3792	5.3	2.1045	7.4	2.1145	12.	2.2674	4.0
5 – 7.5	2.2781	3.1	2.3748	4.3	2.2092	7.0	2.3004	2.4
7.5 – 10	2.5801	2.7	2.4300	3.2	2.4865	5.5	2.5122	1.9
10 – 12.5	2.3393	2.1	2.3827	2.5	2.5263	4.5	2.3775	1.5
12.5 – 15	2.5315	1.9	2.4488	2.2	2.6549	4.0	2.5146	1.3
15 – 20	2.7132	1.1	2.6945	1.4	2.7584	2.3	2.7123	0.8
20 – 25	2.8912	1.0	2.8569	1.2	2.8910	1.9	2.8791	0.7
25 – 30	2.7701	0.8	2.7185	1.0	2.7419	1.6	2.7485	0.6
30 – 40	2.7798	0.6	2.7374	0.8	2.8001	1.1	2.7697	0.5
40 – 50	2.8149	0.6	2.7981	0.8	2.8235	1.1	2.8111	0.5
50 – 60	2.8106	0.6	2.8038	0.8	2.8178	1.1	2.8096	0.5
60 – 80	2.8561	0.5	2.8640	0.7	2.8137	0.9	2.8506	0.4
80 – 100	2.9456	0.5	2.9443	0.7	2.9555	0.8	2.9474	0.4
100 – 120	2.8799	0.6	2.8541	0.8	2.8682	0.8	2.8696	0.4
120 – 150	–	–	–	–	2.6600	0.8	2.6600	0.8
150 – 175	–	–	–	–	2.5561	0.9	2.5561	0.9
175 – 200	–	–	–	–	2.5602	1.0	2.5602	1.0
200 – 225	–	–	–	–	2.5337	1.4	2.5337	1.4
30 – 80	2.8154	0.4	2.8008	0.6	2.8138	0.5	2.8103	0.3

Table 16: $\sigma(^{178}\mathrm{Hf})/\sigma(^{197}\mathrm{Au})$ AND STATISTICAL UNCERTAINTIES (in %)

Energy Bin (keV)	Run I		Run II		Run III		Average	
evaluation 1								
3 – 5	0.4932	11.	0.4467	17.	0.4738	21.	0.4787	8.5
5 – 7.5	0.4101	6.3	0.4476	9.3	0.4316	13.	0.4234	4.9
7.5 – 10	0.5037	4.9	0.4604	6.4	0.5546	8.8	0.4986	3.6
10 – 12.5	0.4666	3.7	0.4527	4.9	0.4507	7.8	0.4602	2.8
12.5 – 15	0.4726	3.2	0.4827	4.1	0.4951	6.4	0.4789	2.3
15 – 20	0.5180	1.8	0.5175	2.5	0.4944	3.8	0.5149	1.4
20 – 25	0.5949	1.5	0.5789	1.9	0.5581	2.9	0.5847	1.1
25 – 30	0.5489	1.2	0.5517	1.6	0.5471	2.4	0.5495	0.9
30 – 40	0.5931	0.9	0.5903	1.3	0.6009	1.6	0.5937	0.7
40 – 50	0.6301	0.9	0.6293	1.3	0.6190	1.6	0.6278	0.7
50 – 60	0.6279	0.9	0.6311	1.2	0.6225	1.5	0.6278	0.6
60 – 80	0.6881	0.8	0.6848	1.1	0.6815	1.2	0.6858	0.6
80 – 100	0.6923	0.8	0.6853	1.1	0.6872	1.1	0.6894	0.6
100 – 120	0.5705	0.9	0.5447	1.2	0.5592	1.2	0.5613	0.6
120 – 150	–	–	–	–	0.5022	1.1	0.5022	1.1
150 – 175	–	–	–	–	0.4650	1.2	0.4650	1.2
175 – 200	–	–	–	–	0.4475	1.4	0.4475	1.4
200 – 225	–	–	–	–	0.4202	2.0	0.4202	2.0
30 – 80	0.6348	0.6	0.6339	1.0	0.6310	0.8	0.6338	0.4
evaluation 2								
3 – 5	0.4009	9.0	0.4105	14.	0.3170	22.	0.3952	7.1
5 – 7.5	0.4030	4.8	0.4243	7.4	0.3716	11.	0.4047	3.8
7.5 – 10	0.4781	3.8	0.4804	4.8	0.4821	7.1	0.4794	2.8
10 – 12.5	0.4679	2.8	0.4486	3.8	0.4198	6.3	0.4564	2.1
12.5 – 15	0.4795	2.5	0.4888	3.1	0.4677	5.3	0.4813	1.8
15 – 20	0.5145	1.5	0.5173	1.9	0.5016	3.0	0.5137	1.1
20 – 25	0.5849	1.2	0.5709	1.5	0.5594	2.3	0.5769	0.9
25 – 30	0.5379	1.0	0.5412	1.3	0.5430	1.9	0.5397	0.7
30 – 40	0.5866	0.7	0.5813	1.0	0.5932	1.3	0.5861	0.5
40 – 50	0.6213	0.7	0.6143	1.0	0.6140	1.3	0.6179	0.5
50 – 60	0.6199	0.7	0.6186	1.0	0.6207	1.3	0.6196	0.5
60 – 80	0.6782	0.6	0.6740	0.8	0.6657	1.0	0.6746	0.4
80 – 100	0.6768	0.6	0.6663	0.8	0.6733	0.9	0.6731	0.4
100 – 120	0.5586	0.7	0.5341	1.0	0.5504	1.0	0.5499	0.5
120 – 150	–	–	–	–	0.4919	1.0	0.4919	1.0
150 – 175	–	–	–	–	0.4538	1.1	0.4538	1.1
175 – 200	–	–	–	–	0.4423	1.2	0.4423	1.2
200 – 225	–	–	–	–	0.4175	1.7	0.4175	1.7
30 – 80	0.6265	0.5	0.6221	0.7	0.6234	0.7	0.6246	0.4

Table 17: $\sigma(^{179}\mathrm{Hf})/\sigma(^{197}\mathrm{Au})$ AND STATISTICAL UNCERTAINTIES (in %)

Energy Bin (keV)	Run I		Run II		Run III		Average	
evaluation 1								
3 – 5	1.3479	9.7	1.4490	12.	1.5164	17.	1.4102	6.8
5 – 7.5	1.2777	5.5	1.4412	7.1	1.4430	11.	1.3540	4.0
7.5 – 10	1.3935	4.8	1.4911	5.1	1.4333	9.0	1.4385	3.3
10 – 12.5	1.3622	3.6	1.4501	4.0	1.1785	8.2	1.3795	2.5
12.5 – 15	1.5136	2.9	1.5349	3.5	1.4467	6.1	1.5136	2.1
15 – 20	1.5401	1.8	1.6257	2.1	1.5264	3.5	1.5688	1.3
20 – 25	1.6974	1.5	1.6862	1.8	1.6355	2.8	1.6849	1.1
25 – 30	1.6692	1.2	1.6821	1.5	1.6597	2.2	1.6720	0.9
30 – 40	1.6286	0.9	1.6370	1.2	1.6499	1.5	1.6350	0.6
40 – 50	1.6798	0.9	1.6800	1.2	1.6981	1.5	1.6833	0.7
50 – 60	1.6560	0.9	1.6588	1.2	1.6528	1.5	1.6562	0.6
60 – 80	1.6849	0.7	1.6869	1.0	1.6805	1.1	1.6845	0.5
80 – 100	1.7212	0.8	1.7619	1.0	1.7564	1.1	1.7404	0.5
100 – 120	1.6996	0.8	1.6988	1.1	1.7424	1.1	1.7115	0.6
120 – 150	–	–	–	–	1.6078	1.0	1.6078	1.0
150 – 175	–	–	–	–	1.5379	1.1	1.5379	1.1
175 – 200	–	–	–	–	1.4989	1.2	1.4989	1.2
200 – 225	–	–	–	–	1.4487	1.8	1.4487	1.8
30 – 80	1.6623	0.6	1.6657	0.9	1.6703	0.7	1.6648	0.4
evaluation 2								
3 – 5	1.4575	6.1	1.4857	7.8	1.6031	12.	1.4876	4.4
5 – 7.5	1.3543	3.8	1.4889	4.8	1.4203	7.5	1.4079	2.7
7.5 – 10	1.4315	3.4	1.5377	3.5	1.5078	6.0	1.4854	2.3
10 – 12.5	1.3937	2.5	1.4570	2.9	1.4471	5.0	1.4248	1.8
12.5 – 15	1.5410	2.2	1.5667	2.4	1.6564	4.3	1.5654	1.5
15 – 20	1.5980	1.3	1.6612	1.6	1.6215	2.6	1.6242	0.9
20 – 25	1.6807	1.1	1.6795	1.3	1.6961	2.1	1.6825	0.8
25 – 30	1.6593	0.9	1.6594	1.1	1.6275	1.7	1.6547	0.7
30 – 40	1.6193	0.7	1.6216	0.9	1.6632	1.2	1.6277	0.5
40 – 50	1.6647	0.7	1.6744	0.9	1.6921	1.2	1.6727	0.5
50 – 60	1.6523	0.7	1.6406	0.9	1.6697	1.2	1.6516	0.5
60 – 80	1.6781	0.6	1.6766	0.8	1.6753	0.9	1.6771	0.4
80 – 100	1.7063	0.6	1.7335	0.8	1.7388	0.9	1.7214	0.4
100 – 120	1.6771	0.7	1.6693	0.9	1.7110	0.9	1.6838	0.5
120 – 150	–	–	–	–	1.5975	0.9	1.5975	0.9
150 – 175	–	–	–	–	1.5121	1.0	1.5121	1.0
175 – 200	–	–	–	–	1.4697	1.1	1.4697	1.1
200 – 225	–	–	–	–	1.4231	1.5	1.4231	1.5
30 – 80	1.6536	0.5	1.6533	0.6	1.6751	0.6	1.6573	0.3

Table 18: $\sigma(^{180}\mathrm{Hf})/\sigma(^{197}\mathrm{Au})$ AND STATISTICAL UNCERTAINTIES (in %)

Energy Bin (keV)	Run I		Run II		Run III		Average	
evaluation 1								
3 – 5	0.2620	20.	0.2071	35.	0.3244	30.	0.2674	15.
5 – 7.5	0.2165	12.	0.2686	15.	0.2831	18.	0.2460	8.2
7.5 – 10	0.1835	12.	0.2245	12.	0.2765	15.	0.2213	7.5
10 – 12.5	0.2416	6.6	0.2399	8.3	0.2538	13.	0.2428	4.8
12.5 – 15	0.2584	5.2	0.2788	6.3	0.2899	9.7	0.2702	3.7
15 – 20	0.2734	3.0	0.2642	4.1	0.2671	6.1	0.2698	2.2
20 – 25	0.3200	2.2	0.3190	2.9	0.3303	4.2	0.3213	1.6
25 – 30	0.2730	2.0	0.2651	2.7	0.2674	3.9	0.2698	1.5
30 – 40	0.2905	1.4	0.2864	2.0	0.3000	2.5	0.2911	1.0
40 – 50	0.3100	1.4	0.3132	2.0	0.3144	2.4	0.3116	1.0
50 – 60	0.3209	1.3	0.3220	1.9	0.3257	2.3	0.3221	1.0
60 – 80	0.3399	1.1	0.3372	1.7	0.3475	1.8	0.3409	0.8
80 – 100	0.3374	1.2	0.3395	1.7	0.3503	1.7	0.3409	0.8
100 – 120	0.2342	1.4	0.2247	2.0	0.2400	1.9	0.2334	1.0
120 – 150	–	–	–	–	0.2061	1.9	0.2061	1.9
150 – 175	–	–	–	–	0.1909	2.0	0.1909	2.0
175 – 200	–	–	–	–	0.1764	2.4	0.1764	2.4
200 – 225	–	–	–	–	0.1710	3.6	0.1710	3.6
30 – 80	0.3153	1.0	0.3147	1.6	0.3219	1.4	0.3164	0.7
evaluation 2								
3 – 5	0.1765	22.	0.1670	33.	0.0733	90.	0.1694	18.
5 – 7.5	0.2029	10.	0.2326	13.	0.1861	22.	0.2108	7.5
7.5 – 10	0.1811	9.8	0.2143	9.9	0.2050	16.	0.1987	6.4
10 – 12.5	0.2387	5.3	0.2203	7.1	0.2099	12.	0.2298	4.0
12.5 – 15	0.2487	4.5	0.2719	5.0	0.2662	8.8	0.2598	3.1
15 – 20	0.2798	2.4	0.2647	3.3	0.2574	5.3	0.2724	1.8
20 – 25	0.3125	1.9	0.3116	2.3	0.3224	3.5	0.3136	1.3
25 – 30	0.2657	1.6	0.2630	2.1	0.2653	3.2	0.2648	1.2
30 – 40	0.2882	1.1	0.2864	1.5	0.2942	2.1	0.2886	0.8
40 – 50	0.3063	1.1	0.3084	1.5	0.3065	2.0	0.3069	0.8
50 – 60	0.3176	1.1	0.3193	1.5	0.3278	1.9	0.3199	0.8
60 – 80	0.3375	0.9	0.3363	1.3	0.3393	1.5	0.3375	0.7
80 – 100	0.3315	0.9	0.3332	1.3	0.3457	1.5	0.3349	0.7
100 – 120	0.2315	1.1	0.2240	1.6	0.2411	1.7	0.2318	0.8
120 – 150	–	–	–	–	0.2030	1.6	0.2030	1.6
150 – 175	–	–	–	–	0.1880	1.8	0.1880	1.8
175 – 200	–	–	–	–	0.1752	2.1	0.1752	2.1
200 – 225	–	–	–	–	0.1757	3.0	0.1757	3.0
30 – 80	0.3124	0.8	0.3126	1.1	0.3170	1.2	0.3132	0.6

Table 19: FINAL NEUTRON CAPTURE CROSS SECTION RATIOS OF ^{176}Hf, ^{177}Hf, ^{178}Hf, ^{179}Hf, AND ^{180}Hf RELATIVE TO ^{197}Au

Energy Bin[a]	$\frac{\sigma(^{176}Hf)}{\sigma(^{197}Au)}$	Uncertainty (%)			$\frac{\sigma(^{177}Hf)}{\sigma(^{197}Au)}$	Uncertainty (%)			$\frac{\sigma(^{178}Hf)}{\sigma(^{197}Au)}$	Uncertainty (%)		
(keV)		stat	sys	tot		stat	sys	tot		stat	sys	tot
3 – 5	0.8308	4.4	1.7	4.7	2.2674	4.0	0.7	4.1	0.3952	7.1	0.7	7.1
5 – 7.5	0.8797	2.5	1.7	3.0	2.3004	2.4	0.7	2.5	0.4047	3.8	0.7	3.9
7.5 – 10	0.9359	2.0	1.7	2.6	2.5122	1.9	0.7	2.0	0.4794	2.8	0.7	2.9
10 – 12.5	0.9765	1.5	1.7	2.3	2.3775	1.5	0.7	1.7	0.4564	2.1	0.7	2.2
12.5 – 15	0.9555	1.4	1.7	2.2	2.5146	1.3	0.7	1.5	0.4813	1.8	0.7	1.9
15 – 20	1.0427	0.9	1.7	1.9	2.7123	0.8	0.7	1.1	0.5137	1.1	0.7	1.3
20 – 25	1.1134	0.7	1.7	1.8	2.8791	0.7	0.7	1.0	0.5769	0.9	0.7	1.1
25 – 30	1.1172	0.6	1.7	1.8	2.7485	0.6	0.7	0.9	0.5397	0.7	0.7	1.0
30 – 40	1.1629	0.5	1.7	1.8	2.7697	0.5	0.7	0.9	0.5861	0.5	0.7	0.9
40 – 50	1.2009	0.5	1.7	1.8	2.8111	0.5	0.7	0.9	0.6179	0.5	0.7	0.9
50 – 60	1.2273	0.5	1.7	1.8	2.8096	0.5	0.7	0.9	0.6196	0.5	0.7	0.9
60 – 80	1.2403	0.4	1.7	1.7	2.8506	0.4	0.7	0.8	0.6746	0.4	0.7	0.8
80 – 100	1.2178	0.4	1.7	1.7	2.9474	0.4	0.7	0.8	0.6731	0.4	0.7	0.8
100 – 120	1.0649	0.4	1.7	1.7	2.8696	0.4	0.7	0.8	0.5499	0.5	0.7	0.9
120 – 150	0.9878	0.8	1.7	1.9	2.6600	0.8	0.7	1.1	0.4919	1.0	0.7	1.2
150 – 175	0.9070	1.0	1.7	2.0	2.5561	0.9	0.7	1.1	0.4538	1.1	0.7	1.3
175 – 200	0.8934	1.1	1.7	2.0	2.5602	1.0	0.7	1.2	0.4423	1.2	0.7	1.4
200 – 225	0.8847	1.5	1.7	2.3	2.5337	1.4	0.7	1.6	0.4175	1.7	0.7	1.8

Energy Bin[a]	$\frac{\sigma(^{179}Hf)}{\sigma(^{197}Au)}$	Uncertainty (%)			$\frac{\sigma(^{180}Hf)}{\sigma(^{197}Au)}$	Uncertainty (%)		
(keV)		stat	sys	tot		stat	sys	tot
3 – 5	1.4876	4.4	0.8	4.5	0.1694	18.	0.9	18.
5 – 7.5	1.4079	2.7	0.8	2.8	0.2108	7.5	0.9	7.6
7.5 – 10	1.4854	2.3	0.8	2.4	0.1987	6.4	0.9	6.5
10 –12.5	1.4248	1.8	0.8	2.0	0.2298	4.0	0.9	4.1
12.5 – 15	1.5654	1.5	0.8	1,7	0.2598	3.1	0.9	3.2
15 – 20	1.6242	0.9	0.8	1.2	0.2724	1.8	0.9	2.0
20 – 25	1.6825	0.8	0.8	1.1	0.3136	1.3	0.9	1.6
25 – 30	1.6547	0.7	0.8	1.1	0.2648	1.2	0.9	1.5
30 – 40	1.6277	0.5	0.8	0.9	0.2886	0.8	0.9	1.2
40 – 50	1.6727	0.5	0.8	0.9	0.3069	0.8	0.9	1.2
50 – 60	1.6516	0.5	0.8	0.9	0.3199	0.8	0.9	1.2
60 – 80	1.6771	0.4	0.8	0.9	0.3375	0.7	0.9	1.1
80 – 100	1.7214	0.4	0.8	0.9	0.3349	0.7	0.9	1.1
100 – 120	1.6838	0.5	0.8	0.9	0.2318	0.8	0.9	1.2
120 – 150	1.5975	0.9	0.8	1.2	0.2030	1.6	0.9	1.8
150 – 175	1.5121	1.0	0.8	1.3	0.1880	1.8	0.9	2.0
175 – 200	1.4697	1.1	0.8	1.4	0.1752	2.1	0.9	2.3
200 – 225	1.4231	1.5	0.8	1.7	0.1757	3.0	0.9	3.1

[a] Energy bins as used for calculating the Maxwellian averaged cross sections

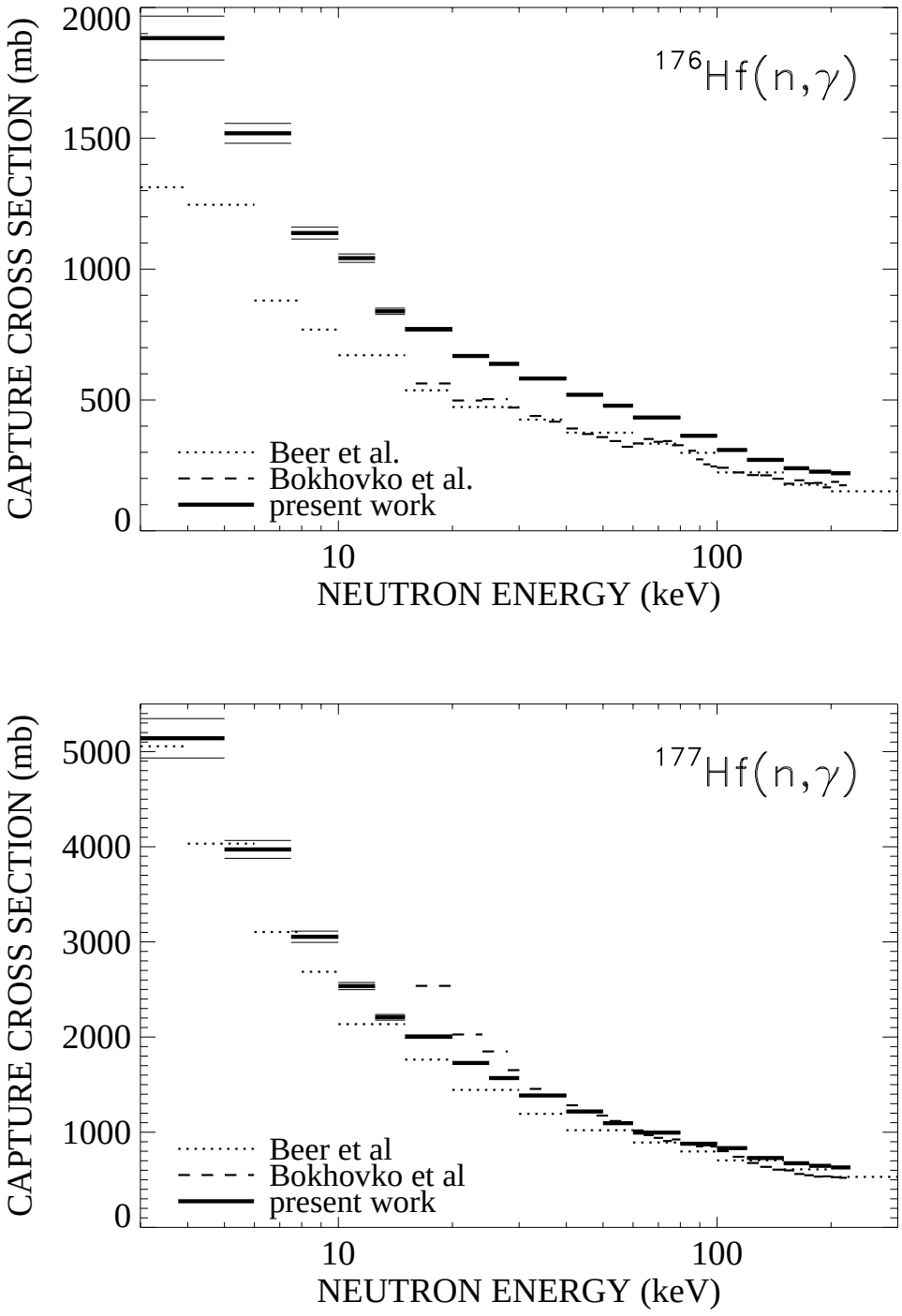

Figure 18: The neutron capture cross sections of ^{176}Hf and ^{177}Hf compared to the data of Beer *et al.* [4] and of Bokhovko *et al.* [12].

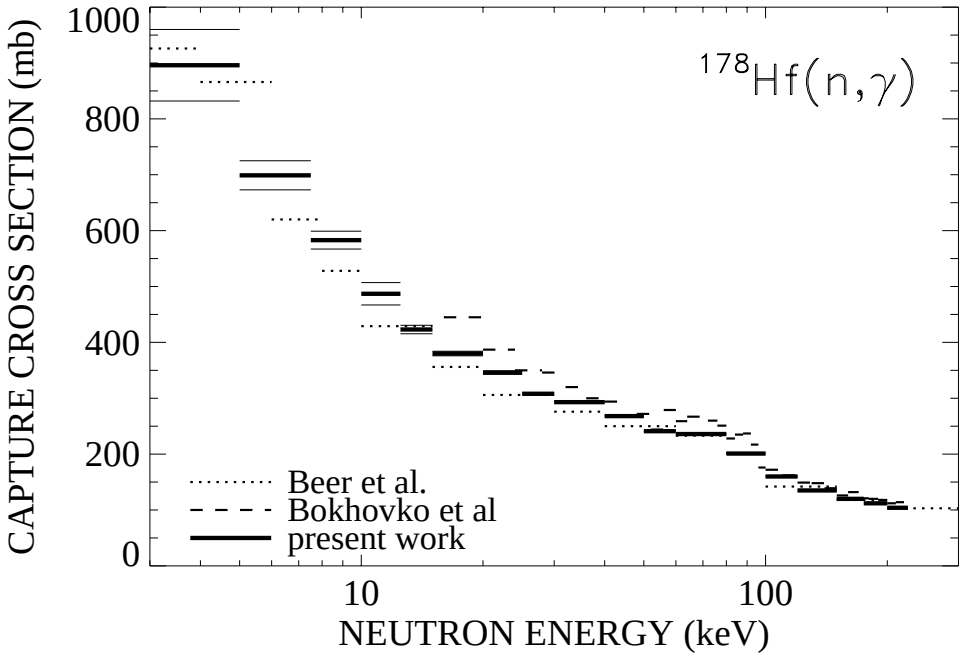

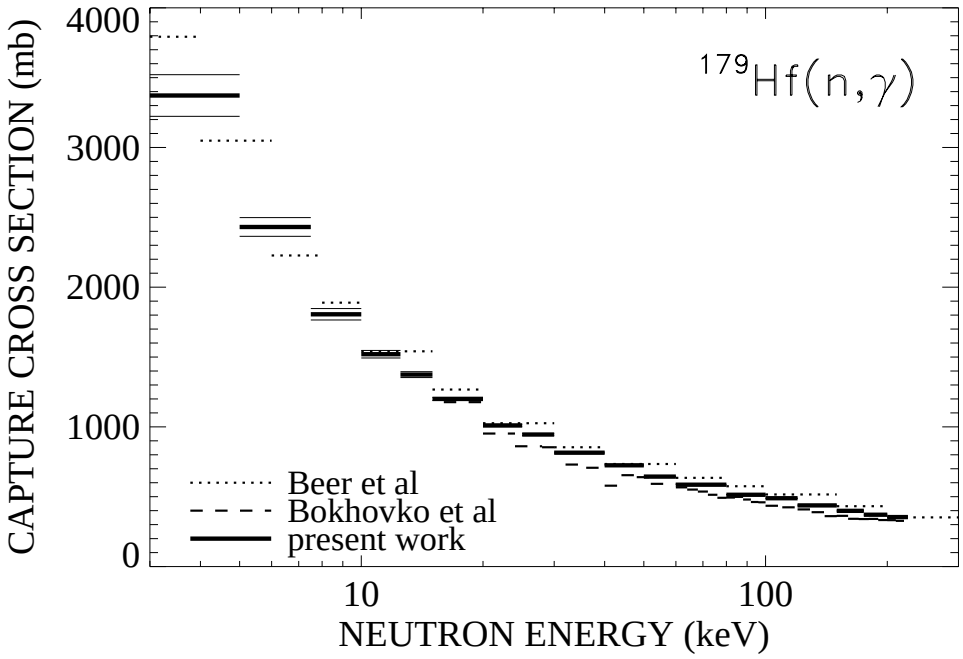

Figure 19: Same as Fig. 18 but for ^{178}Hf and ^{179}Hf.

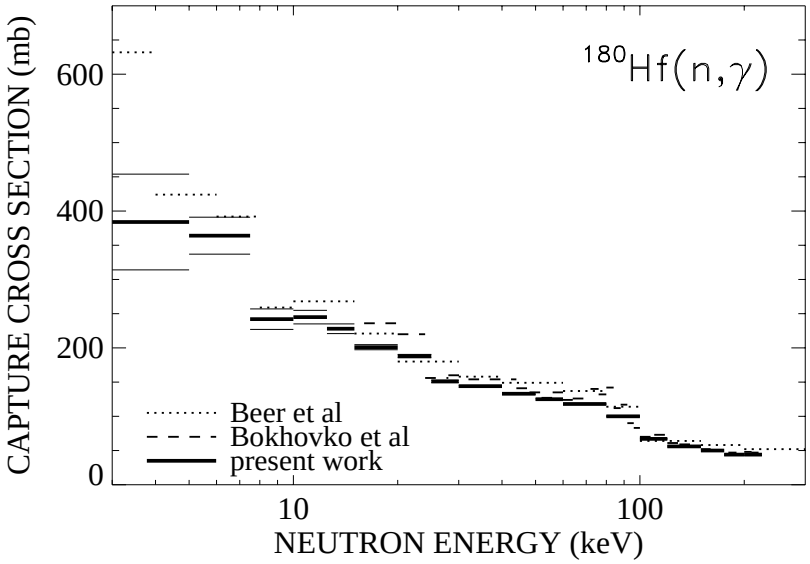

Figure 20: Same as Fig. 18 but for ^{180}Hf.

Table 20: NEUTRON CAPTURE CROSS SECTIONS OF ^{176}Hf, ^{177}Hf, ^{178}Hf, ^{179}Hf, AND ^{180}Hf (in mb).

Energy Bin[a] (keV)	$\sigma(^{197}\mathrm{Au})^b$	$\sigma(^{176}\mathrm{Hf})$	$\sigma(^{177}\mathrm{Hf})$	$\sigma(^{178}\mathrm{Hf})$	$\sigma(^{179}\mathrm{Hf})$	$\sigma(^{180}\mathrm{Hf})$
3 – 5	2266.7	1883.	5140.	895.7	3372.	384.1
5 – 7.5	1726.7	1519.	3972.	698.8	2431.	364.0
7.5 – 10	1215.7	1138.	3054.	582.9	1806.	241.6
10 – 12.5	1066.7	1042.	2536.	486.9	1520.	245.1
12.5 – 15	878.0	839.0	2208.	422.6	1374.	228.1
15 – 20	738.8	770.3	2004.	379.5	1200.	201.2
20 – 25	600.0	668.1	1728.	346.1	1010.	188.2
25 – 30	570.8	637.7	1569.	308.1	944.5	151.1
30 – 40	500.4	581.9	1386.	293.3	814.5	144.4
40 – 50	433.3	520.4	1218.	267.8	724.8	133.0
50 – 60	389.6	478.2	1095.	241.4	643.5	124.6
60 – 80	349.4	433.3	995.9	235.7	585.9	117.9
80 – 100	298.3	363.3	879.2	200.8	513.5	99.9
100 – 120	290.1	309.0	832.6	159.6	488.5	67.3
120 – 150	274.1	270.8	729.2	134.8	437.9	55.7
150 – 175	263.7	239.1	673.9	119.6	398.7	49.6
175 – 200	252.6	225.7	646.6	111.7	371.2	44.2
200 – 225	248.5	219.8	629.5	103.7	353.6	43.7

[a] As used for calculating the Maxwellian averaged cross sections
[b] Based on the ^{197}Au data of Ref. [36] normalized to the activation of Ref. [37]

6 DISCUSSION OF UNCERTAINTIES

Since the determination of statistical and systematic uncertainties in measurements with the 4π BaF_2 detector has been described in detail in Refs. [13, 14, 16], the following discussion concentrates on the particular aspects of the present experiment. The various uncertainties are compiled in Table 21.

The binding energy for all hafnium isotopes is sufficiently low for normalizing the scattering background in the sum energy region around 9 MeV. Therefore, no systematic differences were observed in the data, neither between individual runs nor correlated with the different acquisition modes or evaluation methods (see Tables 14 to 18). Accordingly, systematic uncertainties in background subtraction were negligible as in the measurements on samarium [13], gadolinium [20], and dysprosium [23].

The minor systematic uncertainties related to the flight path measurement and the neutron flux normalization have been discussed previously.

The samples were slightly contaminated by several other metals at the level of about 50 ppm, but the total contamination was less than 0.06% in all cases. Since most of these elements were known to have smaller capture cross sections than Hf, a systematic uncertainty of 0.1% was sufficient to account for these impurities.

For each sample the isotopic composition (Table 2) was specified with an absolute uncertainty of $\pm 0.2\%$ for the main isotope and of $\pm 0.1\%$ for the impurity isotopes. Though these seem to be rather conservative numbers [38] they were adopted in data analysis, resulting in a relative uncertainty of 0.2% for the mass of the main isotopes in the highly enriched samples. For the less enriched ^{176}Hf sample, however, an uncertainty of 0.3% had to be assumed instead.

The uncertainty related to the isotopic correction has been discussed in detail elsewhere [23, 20]. For the isotope with the largest correction ^{176}Hf the uncertainty of the isotopic correction can directly evaluated from the spectra shown in Fig. 6. In the energy range between the threshold at 1.6 MeV and the sum energy peak at 7.1 MeV, which is used for the determination of the ^{176}Hf cross section, the uncorrected spectrum in the upper left corner consists of contributions from captures in ^{176}Hf (61.1%), ^{177}Hf (31.3%), ^{178}Hf (1.9%), ^{179}Hf (2.3%), ^{180}Hf (1.1%) and from scattered neutrons (2.3%). These fractions were derived from the respective sum energy spectra of the other samples. With absolute uncertainties of 0.2% for the main isotope and of 0.1% for each of the four impurities one obtains a total uncertainty of 0.5% for this correction.

As discussed in Sec. 3, the correction for the ^{177}Hf impurity in the ^{176}Hf sample deduced via the isotope matrix of Table 6 led to an overcompensation of this effect. After renormalization, the modified correction factors differed by 2% from the mean of the individual runs. According to this spread an additional systematic uncertainty of 1% was considered for the isotopic correction of the ^{176}Hf sample. In all other samples, no such systematic differences were observed, giving rise to uncertainties of only 0.2%.

Samples with low enrichment are also problematic with respect to the correction for multiple scattering and self-shielding. Subtraction of the normalized spectra of the impurity isotopes may either be insufficient or may even overcompensate the multiple scattering effect. This holds certainly if the individual sample masses are significantly different as it was the case for the ^{176}Hf sample. The overcompensation was clearly visible in the sum

energy spectra and required the renormalization of this correction (Sec.3). For all other samples this effect was not visible in the spectra but may still cause a small uncertainty. Therefore, the calculation of the correction factors MS were performed twice, before and after the correction for isotopic impurities. The respective differences were 1.5% for the ^{176}Hf sample, 0.7% for the ^{179}Hf sample, and less than 0.4% in all other cases, nearly independent of neutron energy. In anology to the gadolinium and dysprosium experiments [20, 23] 25% of this difference were adopted as the related additional uncertainty and were added to the uncertainties provided by the SESH code [17].

The detailed discussion of the systematic uncertainties due to the fraction f of events below the detection threshold for the gadolinium experiment [20] showed that uncertainties of the correction factor F_1 were 0.3% for even and 0.8% for odd isotopes. These corrections were based on two independent sets of calculated capture cascades, and were found to agree with the respective uncertainties quoted in previous measurements with the 4π BaF_2 detector [13, 14, 35]. It turned out that this uncertainty was mainly determined by the difference in binding energy between the investigated isotope and the gold standard, which is large for the odd, but small for the even isotopes. This result was verified by using experimental γ-ray cascades from capture on various dysprosium isotopes [23] and further confirmed in recent analyses of experimental data on ytterbium [10] and cadmium [39] isotopes.

Different from the previous cases, the hafnium isotopes exhibit comparably similar binding energy relative to gold, even for the odd isotopes. Therefore, a constant systematic uncertainty of 0.5% has been adopted for all hafnium isotopes. This uncertainty is also supported by the GEANT simulations, which yield correction factors F_1 (Table 13) that agree on average within 0.8% with the results listed in Table 8.

7 MAXWELLIAN AVERAGED CROSS SECTIONS

Maxwellian averaged cross sections were calculated in the same way as described in Refs. [14, 16]. The neutron energy range from 0 to 700 keV was divided into three intervals I_x according to the origin of the adopted cross sections (see Table 22). The dominant part, I_2, between 3keV and 225 keV is provided by the present experiment (Table 20). These data were obtained with sufficient resolution in neutron energy to exclude systematic uncertainties that may result in the calculation of the Maxwellian average if the energy grid is too coarse.

The contribution I_1 was determined by normalizing the cross sections of Kopecky *et al.* [40] to the present data between 3 keV and 15 keV. The shape of both data sets were found in good agreement, yielding consistent normalization constants in the five energy bins considered. Accordingly, an uncertainty of 5% was obtained for the contribution I_1.

At typical *s*-process temperatures the energy interval I_3 from 225 to 700 keV contributes very little to the Maxwellian average. For this part, the data of Kopecky *et al.* [40] were normalized to the present results between 50 and 225 keV, and the corresponding uncertainties were assumed to increase from 2% at 225 keV to 10% at 700 keV.

Table 21: SYSTEMATIC UNCERTAINTIES (in %)

Flight path	0.1
Neutron flux normalization	0.2
Sample mass: elemental impurities	0.1
Isotopic composition (^{177,178,179,180}Hf/ ^{176}Hf)	0.2/0.3
Isotopic correction (^{177,178,179,180}Hf/ ^{176}Hf)	0.2/1.5
Multiple scattering and self–shielding: F_2	
cross section ratio (^{176}Hf/^{177}Hf/^{178}Hf/^{179}Hf/^{180}Hf)	0.6/0.3/0.4/0.5/0.7
Undetected events: F_1	
cross section ratio	0.5
total systematic uncertainties	
$\sigma(^{176}\mathrm{Hf})/\sigma(\mathrm{Au})$	1.7
$\sigma(^{177}\mathrm{Hf})/\sigma(\mathrm{Au})$	0.7
$\sigma(^{178}\mathrm{Hf})/\sigma(\mathrm{Au})$	0.7
$\sigma(^{179}\mathrm{Hf})/\sigma(\mathrm{Au})$	0.8
$\sigma(^{180}\mathrm{Hf})/\sigma(\mathrm{Au})$	0.9

The systematic uncertainties of the Maxwellian averaged cross sections are determined by the uncertainties of the measured cross section ratios in the interval I_2 and of the respective contributions, I_1 and I_3. The 1.5% uncertainty of the gold standard was not included since it cancels out in most applications of relevance for *s*-process studies. In general, the systematic uncertainties dominate over the statistical uncertainties, except for some isotopes at low thermal energies.

The present results at $kT = 30$ keV are compared in Table 23 with the data obtained in previous experiments [4, 11, 12]and with those recommended in the compilations of Bao *et al.* [1] and Beer, Voss, and Winters [41]. For ^{177,178,179}Hf the new results are very close to the average of the previous experiments. However, the new results for ^{176}Hf show much larger stellar cross sections, far outside the uncertainties claimed for the older data. In all cases, the accuracy could be significantly improved, a crucial achievement with respect to the astrophysical implications of the present data.

8 ACKNOWLEDGEMENTS

We are indebted to G. Rupp for his invaluable technical assistance which was essential for the success of this work.The hospitality of Forschungszentrum Karlsruhe is gratefully acknowledged by L.K.

Table 22: MAXWELLIAN AVERAGED NEUTRON CAPTURE CROSS SECTIONS OF THE HAFNIUM ISOTOPES.

^{176}Hf							
ΔE	0 - 3 keV	3 - 225 keV	225 - 700 keV	Thermal Spectrum			
Data:	from Ref. [40][a]	this work	from Ref. [40][a]				
kT	I_1	I_2	I_3	$<\sigma v>/v_T$ (mbarn)			
(keV)	(mbarn)	(mbarn)	(mbarn)		stat	sys[b]	tot
8	216.1±10.8	1047.±9.9	0.0	1263.	15.	21.	26.
10	144.4±7.2	967.0±7.6	0.0	1111.	10.	19.	21.
15	68.0±3.4	823.9±4.6	0.0	891.9	5.7	15.	16.
20	39.4±2.0	729.4±3.3	0.0	768.8	3.9	13.	14.
25	25.7±1.3	660.4±2.6	0.3	686.4	2.9	12.	12.
30	18.0±0.9	606.3±2.2	1.2	625.5	2.4	11.	11.
40	10.3±0.5	523.2±1.7	5.8±0.2	539.3	1.8	9.2	9.4
50	6.6±0.3	459.0±1.5	14.8±0.5	480.4	1.6	8.2	8.4
52	6.2±0.3	447.6±1.4	17.0±0.5	470.8	1.5	8.0	8.1
60	4.6±0.2	406.0±1.3	27.0±0.9	437.6	1.6	7.4	7.6
70	3.4±0.2	361.1±1.2	40.7±1.4	405.2	1.9	6.9	7.1
80	2.6±0.1	322.5±1.1	54.7±2.0	379.8	2.3	6.5	6.9
90	2.1±0.1	289.3±1.0	68.1±2.6	359.5	2.8	6.1	6.7
100	1.7±0.1	260.6±0.9	80.4±3.3	342.7	3.4	5.8	6.7
^{177}Hf							
ΔE	0 - 3 keV	3 - 225 keV	225 - 700 keV	Thermal Spectrum			
Data:	from Ref. [40][a]	this work	from Ref. [40][a]				
kT	I_1	I_2	I_3	$<\sigma v>/v_T$ (mbarn)			
(keV)	(mbarn)	(mbarn)	(mbarn)		stat	sys[b]	tot
8	541.1±27.	2716.±25.	0.0	3257.	37.	23.	44.
10	361.5±18.	2487.±19.	0.0	2849.	26.	20.	33.
15	170.2±8.5	2079.±11.	0.0	2249.	14.	16.	21.
20	98.6±4.9	1817.±8.2	0.1	1916.	9.6	13.	16.
25	64.2±3.2	1634.±6.5	0.8	1699.	7.2	12.	14.
30	45.1±2.3	1496.±5.4	3.1±0.1	1544.	5.9	11.	12.
40	25.8±1.3	1294.±4.2	15.6±0.4	1335.	4.4	9.3	10.
50	16.6±0.8	1143.±3.6	39.4±1.2	1199.	3.9	8.4	9.3
52	15.4±0.8	1116.±3.5	45.2±1.4	1177.	3.9	8.2	9.1
60	11.6±0.6	1018.±3.2	70.9±2.3	1101.	4.0	7.7	8.7
70	8.6±0.4	910.8±2.9	105.6±3.6	1025.	4.6	7.2	8.5
80	6.6±0.3	818.1±2.7	140.3±5.0	965.0	5.7	6.8	8.9
90	5.2±0.3	737.3±2.5	172.8±6.5	915.3	7.0	6.4	9.5
100	4.2±0.2	666.7±2.3	201.8±7.9	872.7	8.2	6.1	10.

Table 22 (continued)

^{178}Hf							
ΔE	0 - 3 keV	3 - 225 keV	225 - 700 keV	Thermal Spectrum			
Data:	from Ref. [40][a]	this work	from Ref. [40][a]				
kT	I_1	I_2	I_3	$<\sigma v>/v_T$ (mbarn)			
(keV)	(mbarn)	(mbarn)	(mbarn)		stat	sys[b]	tot
8	122.7±6.1	509.9±7.2	0.0	632.6	9.4	4.4	10.
10	81.7±4.1	473.9±5.4	0.0	555.6	6.8	3.9	7.8
15	38.3±1.9	408.9±3.2	0.0	447.2	3.7	3.1	4.8
20	22.2±1.1	365.8±2.2	0.0	388.0	2.5	2.7	3.7
25	14.4±0.7	333.9±1.7	0.1	348.4	1.8	2.4	3.0
30	10.1±0.5	308.2±1.4	0.5	318.8	1.5	2.2	2.7
40	5.8±0.3	267.7±1.1	2.6±0.1	276.1	1.1	1.9	2.2
50	3.7±0.2	235.4±0.9	6.5±0.2	245.6	0.9	1.7	1.9
52	3.5±0.2	229.6±0.9	7.5±0.2	240.6	0.9	1.7	1.9
60	2.6±0.1	208.3±0.8	11.8±0.4	222.7	0.9	1.5	1.7
70	1.9±0.1	185.2±0.7	17.7±0.6	204.8	0.9	1.4	1.7
80	1.5±0.1	165.3±0.7	23.7±0.9	190.5	1.1	1.3	1.7
90	1.2±0.1	148.2±0.6	29.4±1.1	178.8	1.3	1.2	1.8
100	1.0±0.1	133.3±0.6	34.6±1.4	168.9	1.5	1.2	1.9
^{179}Hf							
ΔE	0 - 3 keV	3 - 225 keV	225 - 700 keV	Thermal Spectrum			
Data:	from Ref. [40][a]	this work	from Ref. [40][a]				
kT	I_1	I_2	I_3	$<\sigma v>/v_T$ (mbarn)			
(keV)	(mbarn)	(mbarn)	(mbarn)		stat	sys[b]	tot
8	363.4±18.	1657.±18.	0.0	2020.	25.	16.	30.
10	242.6±12.	1510.±13.	0.0	1753.	18.	14.	23.
15	114.1±5.7	1251.±8.0	0.0	1365.	9.8	11.	15.
20	66.1±3.3	1088.±5.6	0.1	1154.	6.5	9.2	11.
25	43.0±2.2	975.0±4.4	0.4	1018.	4.9	8.1	9.5
30	30.2±1.5	890.7±3.6	1.5	922.4	3.9	7.4	8.4
40	17.2±0.9	768.0±2.8	7.5±0.2	792.7	2.9	6.3	6.9
50	11.1±0.6	676.5±2.4	18.6±0.5	706.2	2.5	5.6	6.1
52	10.3±0.5	660.4±2.3	21.3±0.6	692.0	2.4	5.5	6.0
60	7.8±0.4	601.5±2.1	33.0±1.0	642.3	2.4	5.1	5.6
70	5.7±0.3	537.7±1.9	48.5±1.6	591.9	2.5	4.7	5.3
80	4.4±0.2	482.4±1.8	63.6±2.2	550.4	2.8	4.4	5.2
90	3.5±0.2	434.4±1.6	77.5±2.8	515.4	3.2	4.1	5.2
100	2.8±0.1	392.5±1.5	89.7±3.4	485.0	3.7	3.9	5.4

Table 22 (continued)

^{180}Hf							
ΔE	0 - 3 keV	3 - 225 keV	225 - 700 keV	Thermal Spectrum			
Data:	from Ref. [40][a]	this work	from Ref. [40][a]				
kT	I_1	I_2	I_3	$<\sigma v>/v_T$ (mbarn)			
(keV)	(mbarn)	(mbarn)	(mbarn)		stat	sys[b]	tot
8	43.1±2.2	250.3±7.5	0.0	293.4	7.8	2.6	8.2
10	28.6±1.4	234.6±5.6	0.0	263.2	5.8	2.4	6.3
15	13.4±0.7	204.3±3.2	0.0	217.7	3.3	2.0	3.9
20	7.7±0.4	182.9±2.1	0.0	190.6	2.1	1.7	2.7
25	5.0±0.3	166.4±1.6	0.1	171.5	1.6	1.5	2.2
30	3.5±0.2	152.8±1.3	0.2	156.5	1.3	1.4	1.9
40	2.0±0.1	131.0±0.9	1.0	134.0	0.9	1.2	1.5
50	1.3±0.1	113.7±0.8	2.6±0.1	117.6	0.8	1.0	1.3
52	1.2±0.1	110.6±0.7	3.0±0.1	114.8	0.7	1.0	1.2
60	0.9±0.0	99.5±0.7	4.7±0.2	105.1	0.7	0.9	1.1
70	0.7±0.0	87.7±0.6	7.0±0.2	95.4	0.6	0.9	1.1
80	0.5±0.0	77.7±0.5	9.4±0.3	87.6	0.6	0.8	1.0
90	0.4±0.0	69.2±0.5	11.6±0.4	81.2	0.6	0.7	0.9
100	0.3±0.0	61.9±0.4	13.6±0.5	75.8	0.6	0.7	0.9

[a]Normalized to present data

[b]The 1.5% uncertainty of the gold standard is not included here, since it cancels out in most applications of relevance for nuclear astrophysics

Table 23: MAXWELLIAN AVERAGED CROSS SECTIONS (in mb) AT $kT = 30$ keV COMPARED TO PREVIOUS EXPERIMENTS AND COMPILATIONS

Isotope	Experimental cross section		Cross Section from compilation	
		Reference	Bao *et al.* [1]	Beer, Voss & Winters [41]
^{176}Hf	625.5 ± 11.	present work[a]	455±20	458±20
	449 ± 27	Bhokovko *et al.* (1992) [12]		
	458 ± 20	Beer *et al.* (1984) [4]		
^{177}Hf	1544. ± 12.	present work[a]	1500±100	1366±61
	1663 ± 83	Bokhovko *et al.* (1992) [12]		
	1366 ± 61	Beer *et al.* (1984) [4]		
^{178}Hf	318.8 ± 2.7	present work[a]	314 ±10	310 ±10
	327 ± 20	Bokhovko *et al.* (1992) [12]		
	310 ± 10	Beer *et al.* (1982) [11]		
^{179}Hf	922.4 ± 8.4	present work[a]	956±50	991 ± 30
	858 ± 43	Bhokovko *et al.* (1992) [12]		
	991 ± 30	Beer *et al.* (82) [11]		
^{180}Hf	156.5 ± 1.9	present work[a]	179 ± 5	175 ± 5
	169 ± 14	Bokhovko *et al.* (1992) [12]		
	179 ± 5	Beer *et al.* (82) [11]		

[a] The 1.5% uncertainty of the gold cross section is not included, since it cancels out in most applications of relevance for nuclear astrophysics.

References

[1] Z.Y. Bao, H. Beer, F. Käppeler, F. Voss, K. Wisshak, and T. Rauscher, Atomic Data Nucl. Data Tables **76**, 70 (2000).

[2] H. Beer, F. Käppeler, K. Wisshak, and R. Ward, Astrophys. J. Suppl. Series **46**, 295 (1981).

[3] N. Klay, f. Käppeler, H. Beer, and G. Schatz, Phys. Rev. C **44**, 2839 (1991).

[4] H. Beer, G. Walter, R.L. Macklin, and P.J. Patchett, Phys. Rev. C **30**, 464 (1984).

[5] K. Wisshak, F. Voss, C. Arlandini, F.Bečvář, O. Straniero, R. Gallino, M. Heil, F. Käppeler, M. Krtička, S. Masera, R. Reifarth, and C. Travaglio, Phys. Rev. Let. **87**, 251102 (2001).

[6] D. Belic *et al.* . Phys. Rev. C **65**, 035801 (2002).

[7] F. Käppeler, C. Arlandini, M. Heil, F. Voss, K. Wisshak, R. Reifarth, O. Straniero, R. Gallino, S. Masera, and C. Travaglio, Phys. Rev. C in print.

[8] F. Voss, K. Wisshak, and F. Käppeler, in *Capture Gamma-Ray Spectroscopy and Related Topics*, edited by S. Wender, AIP Conference Proceedings 529 (AIP, New York, 2000), p. 660.

[9] K. Wisshak, F. Voss, F. Käppeler, M. Krtička, and F.Bečvář, in *Capture Gamma-Ray Spectroscopy and Related Topics*, edited by S. Wender, AIP Conference Proceedings 529 (AIP, New York, 2000), p. 675.

[10] K. Wisshak, F. Voss, C. Arlandini, F. Käppeler, and L. Kazakov, Phys. Rev. C **61**, 065801 (2000).

[11] H. Beer and R.L. Macklin, Phys. Rev. C **26**, 1404 (1982).

[12] M.V. Bokhovko, V.N. Kononov, E.D. Poletaev, N.S. Rabotnov, and V.M. Timokhov, in *Nuclear Data for Science and Technology*, edited by S.M. Qaim (Springer, Berlin, 1992), p. 62.

[13] K. Wisshak, K. Guber, F. Voss, F. Käppeler, and G. Reffo, Phys. Rev. C **48**, 1401 (1993).

[14] K. Wisshak, F. Voss, F. Käppeler, and G. Reffo, Phys. Rev. C **45**, 2470 (1992).

[15] K. Wisshak, K. Guber, F. Käppeler, J. Krisch, H. Müller, G. Rupp, and F. Voss, Nucl. Instr. Meth. A **292**, 595 (1990).

[16] K. Wisshak, F. Voss, F. Käppeler, and G. Reffo, Phys. Rev. C **42**, 1731 (1990).

[17] F. H. Fröhner, Report GA-8380, Gulf General Atomic (1968).

[18] C. Nordborg, H. Gruppelaar, and M. Salvatores, in *Nuclear Data for Science and Technology*, edited by S. Qaim (Springer, Berlin, 1992), p. 782.

[19] V. McLane, C.L. Dunford, and P.F. Rose, in *Neutron Cross Sections, Vol. 2,* (Academic Press, New York, 1988).

[20] K. Wisshak, F. Voss, F. Käppeler, K. Guber, L. Kazakov, N. Kornilov, M. Uhl, and G. Reffo, Phys. Rev. C. **52**, 2762 (1995).

[21] R. Reifarth, M. Heil, F. Käppeler, F. Voss, K. Wisshak, F.Bečvář, M. Krtička, R. Gallino, and Y. Nagai, Phys. Rev. C **66**, 064603 (2002).

[22] K. Wisshak, F. Voss, F. Käppeler, L. Kazakov, and G. Reffo, Report FZKA5967, Forschungszentrum Karlsruhe, Karlsruhe (1997).

[23] F. Voss, K. Wisshak, C. Arlandini,K. Käppeler, L. Kazakov, and T. Rauscher, Phys. Rev. C **59**, 1154 (1999).

[24] A. Gilbert and A.G.W. Cameron, Can. J. Phys. **43**, 1446 (1965).

[25] J. F. Mughabghab, M. Divadeenam, and N. E. Holden, in *Neutron Cross Sections, Vol. 1, Part A* (Academic Press, New York, 1981).

[26] R.B. Firestone, and V. S. Shirley, *Table of Isotopes* 8^{th} Edition, (Wiley, New York, 1996).

[27] J. Apostolakis, Technical Report, CERN, GEANT library (available from: www.cern.ch).

[28] M. Heil, R. Reifarth, M.M. Fowler, R.C. Haight, F. Käppeler, R.S. Rundberg, E.H. Seabury, J.L. Ullmann, J.B. Wilhelmy, and K. Wisshak, Nucl. Instr. Methods **A 459**, 229 (2001).

[29] F. Bečvář, in *Capture Gamma-Ray Spectroscopy and Related Topics*, edited by S. Wender, AIP Conference Proceedings 529 (AIP, New York, 2000), p. 504.

[30] F. Bečvář, Nucl. Instr. Methods **A 417**, 434 (1998).

[31] F.G. Kondev, Nucl. Data Sheets **98**, 801 (2003).

[32] S.C. Wu and H. Niu, Nucl. Data Sheets **100**, 483 (2003).

[33] R.B. Firestone, Nucl. Data Sheets **62**, 101 (1991).

[34] H. Beer, and R.A. Ward, Nature **291**, 308 (1981).

[35] F. Voss, K. Wisshak, K. Guber, F.Käppeler, and G. Reffo, Phys. Rev. C **50**, 2582 (1994).

[36] R. L. Macklin, private communication (unpublished).

[37] W. Ratynski and F. Käppeler, Phys. Rev. C **37**, 595 (1988).

[38] K. Wisshak, F. Voss, F. Käppeler, L. Kazakov, and G. Reffo, Phys. Rev. C. **57**, 391 (1998).

[39] K. Wisshak, F. Voss, F. Käppeler, and L. Kazakov, Phys. Rev. C **66**, 025801 (2002).

[40] J. Kopecky, J.-Ch. Sublet, J.A. Simpson, R.A. Forrest, and D. Nierop, Report INDC(NDS)-362, International Atomic Energy Agency, Vienna, Austria, 1997.

[41] H. Beer, F. Voss, and R.R. Winters, Astrophys. J. Suppl. **80**, 403 (1992).